Axin1 Protects Colon Carcinogenesis by an Immune-Mediated Effect

Romain Sanson, Silvia Luna Lazzara, David Cune, Caterina Luana Pitasi, Coralie Trentesaux, Marie Fraudeau, Franck Letourneur, Benjamin Saintpierre, Morgane Le Gall, Pascale Bossard, et al.

cmgh
CELLULAR AND MOLECULAR GASTROENTEROLOGY AND HEPATOLOGY

ORIGINAL RESEARCH

Axin1 Protects Colon Carcinogenesis by an Immune-Mediated Effect

Romain Sanson,[1,2] Silvia Luna Lazzara,[1,2,*] David Cune,[1,2,*] Caterina Luana Pitasi,[1,2] Coralie Trentesaux,[1,2] Marie Fraudeau,[1,2] Franck Letourneur,[3] Benjamin Saintpierre,[3] Morgane Le Gall,[4] Pascale Bossard,[1,2] Benoit Terris,[1,2,5] Pascal Finetti,[6] François Bertucci,[6] Emilie Mamessier,[6] Béatrice Romagnolo,[1,2,§] and Christine Perret[1,2,§]

[1]Université de Paris, Institut Cochin, INSERM, Centre National Recherche Scientifique, Paris, France; [2]Equipe Labellisée Ligue Nationale Contre Le Cancer, Paris, France; [3]Genomic Facility, Université de Paris, Institut Cochin, INSERM, Centre National Recherche Scientifique, Paris, France; [4]Proteomic Facility, Université de Paris, Institut Cochin, INSERM, Centre National Recherche Scientifique, Paris, France; [5]Assistance Publique Hôpitaux de Paris, Hôpitaux Universitaires Paris Centre, Pathology Department, Hôpital Cochin, Paris, France; and [6]Laboratory of Predictive Oncology, Centre de Recherche en Cancérologie de Marseille, Institut Paoli-Calmettes, INSERM Unité Mixte de Recherche 1068, Centre National Recherche Scientifique Unité Mixte de Recherche 725, Marseille, France

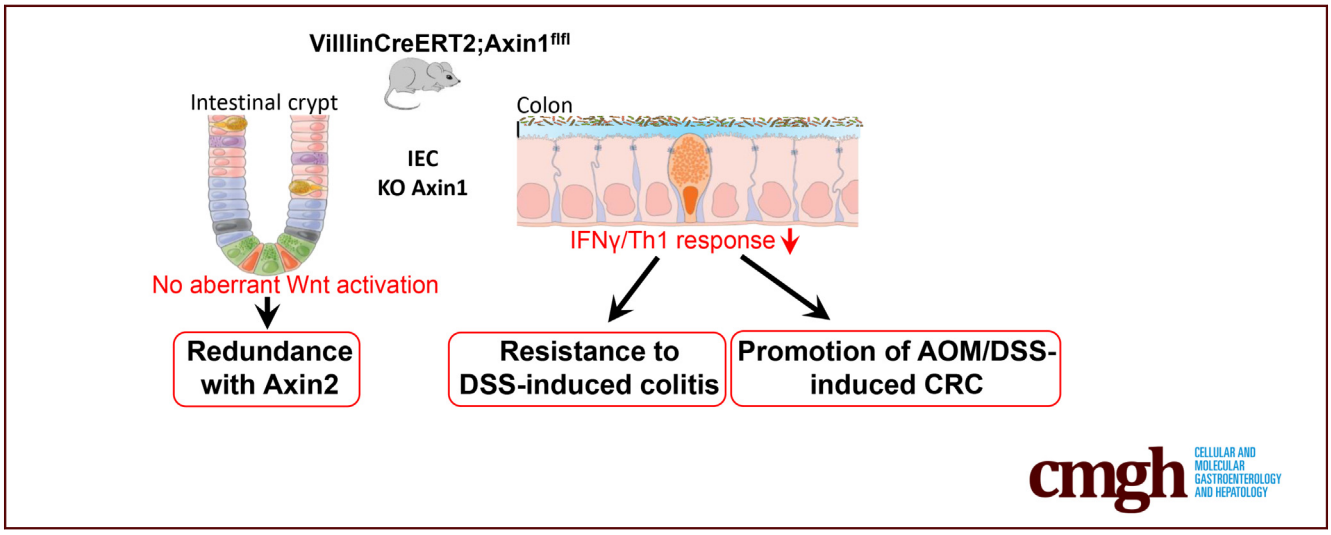

SUMMARY

We show that Axin1, a Wnt/β-catenin partner, has redundant function with Axin2, for Wnt down-regulation in intestine, and identify an unrecognized role of Axin1 in the control of immune inflammation that accounts for its tumor-suppressor function in colorectal tumorigenesis.

BACKGROUND & AIMS: Axin1 is a negative regulator of wingless-type MMTV integration site family, member 1 (Wnt)/β-catenin signaling with tumor-suppressor function. The Wnt pathway has a critical role in the intestine, both during homeostasis and cancer, but the role of Axin1 remains elusive.

METHODS: We assessed the role of Axin1 in normal intestinal homeostasis, with control, epithelial-specific, *Axin1*-knockout mice ($Axin1^{\Delta IEC}$) and *Axin2*-knockout mice. We evaluated the tumor-suppressor function of *Axin1* during chemically induced colorectal tumorigenesis and dextran sulfate sodium–induced colitis, and performed comparative gene expression profiling by whole-genome RNA sequencing. The clinical relevance of the *Axin1*-dependent gene expression signature then was tested in a database of 2239 clinical colorectal cancer (CRC) samples.

RESULTS: We found that *Axin1* was dispensable for normal intestinal homeostasis and redundant with *Axin2* for Wnt pathway down-regulation. *Axin1* deficiency in intestinal epithelial cells rendered mice more susceptible to chemically induced colon carcinogenesis, but reduced dextran sulfate sodium–induced colitis by attenuating the induction of a proinflammatory program. RNA-seq analyses identified an interferon γ/T-helper1 immune program controlled by Axin1 that enhances the inflammatory response and protects against CRC. The *Axin1*-dependent gene expression signature was applied to human CRC samples and identified a group of patients with potential vulnerability to immune checkpoint blockade therapies.

CONCLUSIONS: Our study establishes, in vivo, that Axin1 has redundant function with Axin2 for Wnt down-regulation and infers a new role for Axin1. Physiologically, Axin1 stimulates gut inflammation via an interferon γ/Th1 program that prevents tumor growth. Linked to its T-cell–mediated effect, the colonic *Axin1* signature offers therapeutic perspectives for CRC. *(Cell Mol Gastroenterol Hepatol 2023;15:689–715; https://doi.org/10.1016/j.jcmgh.2022.10.017)*

Keywords: Intestinal Homeostasis; Colon Carcinogenesis; Wnt/β-Catenin Pathway; Axin; Intestinal Inflammation.

Despite the remarkable clinical advances in cancer diagnosis and treatment achieved in recent decades, the mortality rate of colorectal cancer (CRC) remains high worldwide, with almost 600,000 deaths each year.[1] A precise understanding of the molecular mechanisms underlying CRC pathogenesis therefore is crucial for the improvement of therapeutic strategies. Novel targets are emerging in the form of the proteins of the wingless-type MMTV integration site family, member 1 (Wnt)/β-catenin pathway, which is activated in almost all CRCs, mostly through mutations of the *APC* tumor-suppressor gene.[2] However, the therapeutic targeting of this pathway has proved challenging.[3] Improvements in our understanding of the biology of the Wnt/β-catenin pathway therefore are required for the development of new therapeutic opportunities.

Mutations of *APC* are common in CRC, whereas mutations of *AXIN1*, a gene encoding another component of the Wnt pathway, are infrequent in these cancers.[4] The potential tumor-suppressor function of Axin1 in CRC remains unclear, but compounds stabilizing this protein have been reported to suppress the growth of Wnt-driven CRCs.[5,6] By contrast, a tumor-suppressor function for Axin1 has been shown clearly in hepatocellular carcinoma (HCC), for which *AXIN1* mutations are identified in almost 10% of cases.[7] It has been suggested that these mutations are associated with the role of Axin1 in the down-regulation of Wnt/β-catenin signaling.[8] However, most human HCCs with *AXIN1* mutations studied have not been found to be associated with higher levels of β-catenin activation, and the HCCs developing in mice with *Axin1* inactivation in hepatocytes do not display aberrant activation of the Wnt pathway.[9]

Nevertheless, Axin1 initially was identified as a negative regulator of the canonical Wnt pathway.[10,11] Several lines of evidence indicate that Axin1 and its homolog Axin2 play a key role in down-regulating the stability of β-catenin, encoded by *Ctnnb1*, which is crucial for the cellular response Wnt/β-catenin signaling.[12] In the absence of the Wnt signal, Axins act as scaffold proteins, together with the tumor-suppressor Adenomatous polyposis coli, in the destruction complex targeting β-catenin for degradation. However, Axin1 also is involved in transducing the Wnt signal, leading to an increase in cytoplasmic and nuclear β-catenin levels and the expression of β-catenin target genes.[12] Axin1 also acts as a scaffold protein for other non-Wnt pathways, including the c-Jun N-terminal kinase, transforming growth factor-β, p53, and AMP-activated protein kinase pathways.[13,14]

Given the complex functions of Axin1, we decided to investigate its role in normal intestinal homeostasis and its tumor-suppressor function in CRC. Using mice with an epithelium-specific inactivation of *Axin1*, we showed that *Axin1* was dispensable for normal intestinal homeostasis and redundant with *Axin2* for down-regulation of the Wnt pathway. Mice that have combined deficiencies for *Axin1* and *Axin2* phenocopied *Apc*-deficient mice. We found that *Axin1* deficiency in intestinal epithelial cells promoted the development of azoxymethane (AOM)-induced colon tumorigenesis, but induced an improvement of dextran sulfate sodium (DSS)-induced colitis. Axin1 therefore promotes an inflammatory program with tumor-suppressor function in intestinal epithelial cells that we identified as an interferon (IFN)γ/helper T cell 1 (Th1) immune program. We defined an *Axin1*-dependent gene expression signature (GES), which we then used to probe databases of human CRC transcriptomes. Patients with tumor profiles defined by the signature as *Axin1*-deficient had poor antitumor immune response and poor clinical outcome, whereas those with the *Axin1*-proficient profile had a better survival and an immune profile of potential vulnerability to immune checkpoint blockade therapies.

Results

Axin1 *Is Not Required for Homeostasis in the Intestinal Epithelium, but Its Loss Sensitizes Progenitors to the Toxicity Resulting From Tamoxifen-inducible Cre Recombinase Activation*

For assessment of the function of Axin1 in the intestine, we generated an *Axin1*-conditional knockout mouse strain under the control of the villin promoter (Vil CreER^{T2};Axin1$^{fl/fl}$, referred to hereafter as Axin1$^{\Delta \text{Intestinal Epithelial Cell [IEC]}}$), in which *Axin1* selectively was inactivated in all

***Authors share co-second authorship; §Authors share co-senior and co-corresponding authorship.**

Abbreviations used in this paper: **Apc, Adenomatous polposis Coli; AOM, azoxymethane; CMS, consensus molecular subtype; CRC, colorectal cancer; CreER^{T2}, tamoxifen-inducible Cre recombinase; DEG, differentially expressed gene; DFS, disease-free survival; DKO, double-knockout; DSS, dextran sulfate sodium; Gapdh, glyceraldehyde-3-phosphate dehydrogenase; GES, gene expression signature; GSEA, gene set enrichment analysis; HCC, hepatocellular carcinoma; IEC, Intestinal epithelial Cell; IFN, interferon; IL, interleukin; IP, intraperitoneal; KO, knockout; NF-κB, nuclear factor-κB; PBS, phosphate-buffered saline; pMMR, proficient mismatch repair; qRT-PCR, quantitative reverse-transcription polymerase chain reaction; RNA-seq, RNA sequencing; STAT, signal transducer and activator of transcription; Th1, helper T cell 1; TNF, tumor necrosis factor; TRITC, tetramethylrhodamine B isothiocyanate; TUNEL, terminal deoxynucleotidyl transferase–mediated deoxyuridine triphosphate nick-end labeling; Wnt, wingless-type MMTV integration site family, member 1; WT, wild-type.**

Most current article

2352-345X
https://doi.org/10.1016/j.jcmgh.2022.10.017

intestinal epithelial cells. Control (Axin1$^{fl/fl}$ or Vil CreER^{T2};Axin1$^{+/+}$) and Axin1$^{\Delta IEC}$ mice were subjected to 4 daily intraperitoneal (IP) injections of tamoxifen, and were analyzed on day 5 postinduction. Western blot confirmed the absence of Axin1 in the small intestine and colon of Axin1$^{\Delta IEC}$ mice, and its presence in these tissues in control mice (Figures 1*A* and 2*A*). Histologic analyses were performed on the small intestine and colon of mutant and control mice. Mutant mice showed no major change in intestinal architecture or cell fate relative to controls (Figures 1*B–E*, 2*B–E*, and 3). However, H&E staining showed the presence of numerous apoptotic cells in the crypts of the small intestine of Axin1$^{\Delta IEC}$ mice. This finding was confirmed by active caspase-3 and terminal deoxynucleotidyl transferase–mediated deoxyuridine triphosphate nick-end labeling (TUNEL) staining, revealing significantly larger numbers of cleaved caspase-3-positive and TUNEL-positive cells in the crypt in Axin1$^{\Delta IEC}$ mice than in controls (Figure 1*C* and *D*). A similar increase in the number of cleaved caspase-3-positive and TUNEL-positive cells relative to controls was observed in the colon of Axin1$^{\Delta IEC}$ mice (Figure 2*C* and *D*). We analyzed proliferation status in the small intestine and colon of Axin1$^{\Delta IEC}$ mice. We found that the number of proliferating cells in these compartments of the mutant mice was no higher than that in control mice (Figures 1*E* and 2*E*).

Surprisingly, we found that the apoptotic phenotype observed in the crypt of Axin1$^{\Delta IEC}$ mice mostly concerned progenitor cells and was transient (Figure 4). It disappeared 15 days postinduction, although Western blot continued to confirm the absence of Axin1 in the intestine of mutant mice (Figure 1*F* and *G*). We investigated the possibility that apoptosis might result from a sensitivity of *Axin1*-deficient crypts to the toxicity induced by CreER^{T2} activation because apoptosis levels were significantly higher in the crypts of control (Vil CreER^{T2};Axin1$^{+/+}$) mice than in those of control Axin1$^{fl/fl}$ mice, although still much lower than those observed for Axin1$^{\Delta IEC}$ mice (Figure 1*C* and *D*). Such toxicity has been described elsewhere.[15] Mutant and control mice were treated with 2 daily doses of tamoxifen and were killed on days 3 and 8 postinduction. The apoptosis observed on day 3 in mutant mice was transient and had disappeared by day 8 (Figure 4*B*). We also tested the effect of a new IP tamoxifen treatment and confirmed that tamoxifen reinjection induced de novo apoptosis in the crypts of Axin1$^{\Delta IEC}$ mice (Figure 4*C*). Consistent with Cre genotoxicity, γH2AX foci were observed in the crypts of mutant mice at day 5 postinduction, and were associated with an accumulation of nuclear p53 (Figure 4*D*). Consistent with these data, the crypts of mice with intestinal epithelial cells deficient for both *Axin1* and *p53* (Vil CreER^{T2};Axin1$^{fl/fl}$;p53$^{fl/fl}$) had significantly fewer apoptotic cells on day 5 postinduction than the crypts of mice lacking only *Axin1* (Figure 4*E*).

Our results show that *Axin1* is dispensable for normal homeostasis of the intestinal epithelium but that its loss sensitizes crypt progenitors to the genotoxicity induced by CreER^{T2} activation.

Axin2 *Compensates for the Loss of* Axin1 *in the Control of Wnt/β-Catenin Signaling*

The absence of hyperproliferation of the crypt cells in Axin1$^{\Delta IEC}$ mice suggested that *Axin1* inactivation in the intestinal epithelium did not lead to an aberrant activation of Wnt/β-catenin signaling. We tested this hypothesis by quantitative reverse-transcription polymerase chain reaction (qRT-PCR) analysis of the expression of 2 canonical β-catenin target genes: *Axin2* and *Lgr5*. The levels of *Axin2* and *Lgr5* expression in the various parts of the small intestine and colon did not differ significantly between mutant mice and controls (Figure 5*A*). We hypothesized that functional redundancy with *Axin2* might account for the lack of phenotype of Axin1$^{\Delta IEC}$ mice. We crossed these mice with *Axin2*-null mice with *lacZ* knock-in alleles,[16] referred to here as Axin2 knockout (KO) mice. Histologic analyses showed no disturbance to the architecture and cell proliferation of the small intestine and colon in these mice (Figures 5*C–E* and 6*A–C*). By contrast, mice with invalidations of both *Axin1* and *Axin2* in the intestinal epithelium (Vil CreER^{T2};Axin1$^{fl/fl}$;Axin2^{lacZ,lacZ}), hereafter referred to as double-knockout (DKO) mice, had a severe intestinal phenotype mimicking that observed after *Apc* inactivation in the intestinal epithelium.[17] These Vil CreER^{T2};Apc$^{fl/fl}$ mice are referred to hereafter as Apc$^{\Delta IEC}$ mice. DKO mice, similar to Apc$^{\Delta IEC}$ mice, died within 7 days of tamoxifen injection (Figure 5*B*), whereas Axin1$^{\Delta IEC}$ and Axin2KO mice remained alive for at least 1 year after injection (Figure 5*B* and data not shown). Likewise, H&E analyses of the small intestine showed an enlargement of the crypt in DKO mice resembling that observed in Apc$^{\Delta IEC}$ mice[17] (Figure 5*C*). This enlargement was associated with a large increase in the number of proliferating and apoptotic cells in the crypts of DKO mice that was not observed in the crypts of mice lacking only *Axin1* or *Axin2* or in controls, except for the small transient increase in apoptosis observed in Axin1$^{\Delta IEC}$ mice (Figures 1*B* and 5*D* and *E*). An increase in the number of Olfm4-positive cells was observed, highlighting an increase in the intestinal stem cell compartment (Figure 5*F*). Furthermore, we observed a mislocalization of Paneth cells in the DKO mice. These cells were scattered throughout the enlarged crypts, rather than being confined to the bottom of the crypt, as observed for control mice and mice lacking either *Axin1* or *Axin2* (Figure 5*G*). All of these histologic features mimicked the characteristics of Apc$^{\Delta}$IEC mice.[17] A phenocopy of Apc$^{\Delta IEC}$ mice also was observed in the colon of DKO mice, with an increase in the crypt length, apoptosis and cell proliferation, and de novo expression of the Paneth cell marker lysozyme[17] (Figure 6).

We then performed qRT-PCR to analyze the expression of several β-catenin target genes in the small intestine and colon of DKO, control, and mice deficient for *Axin1* or *Axin2*. *Axin2* expression did not increase significantly in *Axin1*-deficient mice, and vice versa (Figure 7), excluding any compensation of expression between these 2 genes. More importantly, the results confirmed the aberrant activation of Wnt/β-catenin signaling in DKO mice, with strong induction observed for several β-catenin target genes (*c-myc*, *Ascl2*, *Sp5*, *Sox9*, *Ephb3*) in both the small intestine and colon, as reported for *Apc*-deficient mice.[17] The lack of induction of

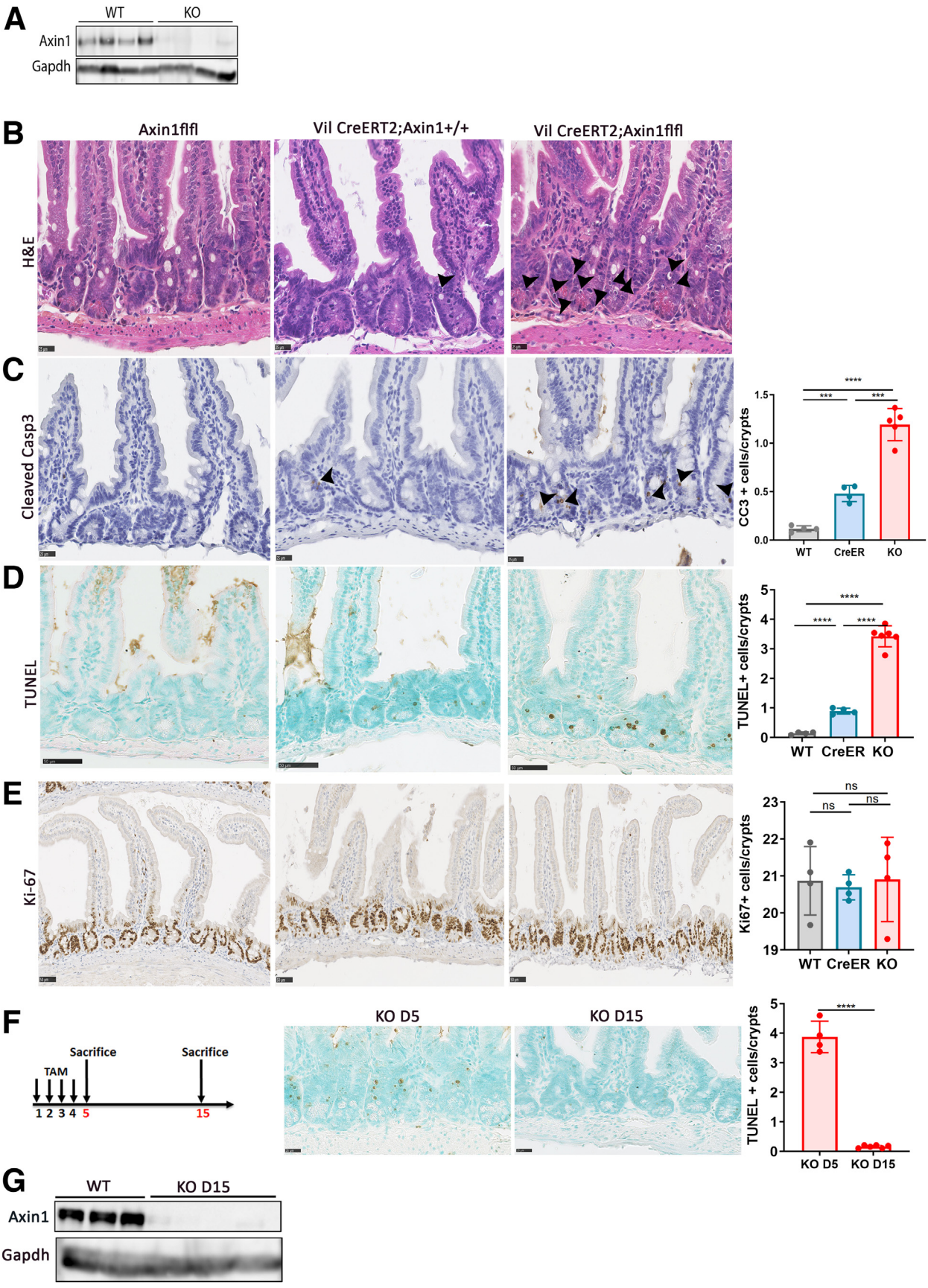
A
WT
KO
Axin1
Gapdh
B
Axin1flfl
Vil CreERT2;Axin1+/+
Vil CreERT2;Axin1flfl
H&E
C
Cleaved Casp3
CC3 + cells/crypts
WT
CreER
KO
D
TUNEL
TUNEL+ cells/crypts
E
Ki-67
Ki67+ cells/crypts
ns
F
Sacrifice
Sacrifice
TAM
1 2 3 4 5
15
KO D5
KO D15
TUNEL + cells/crypts
G
WT
KO D15
Axin1
Gapdh

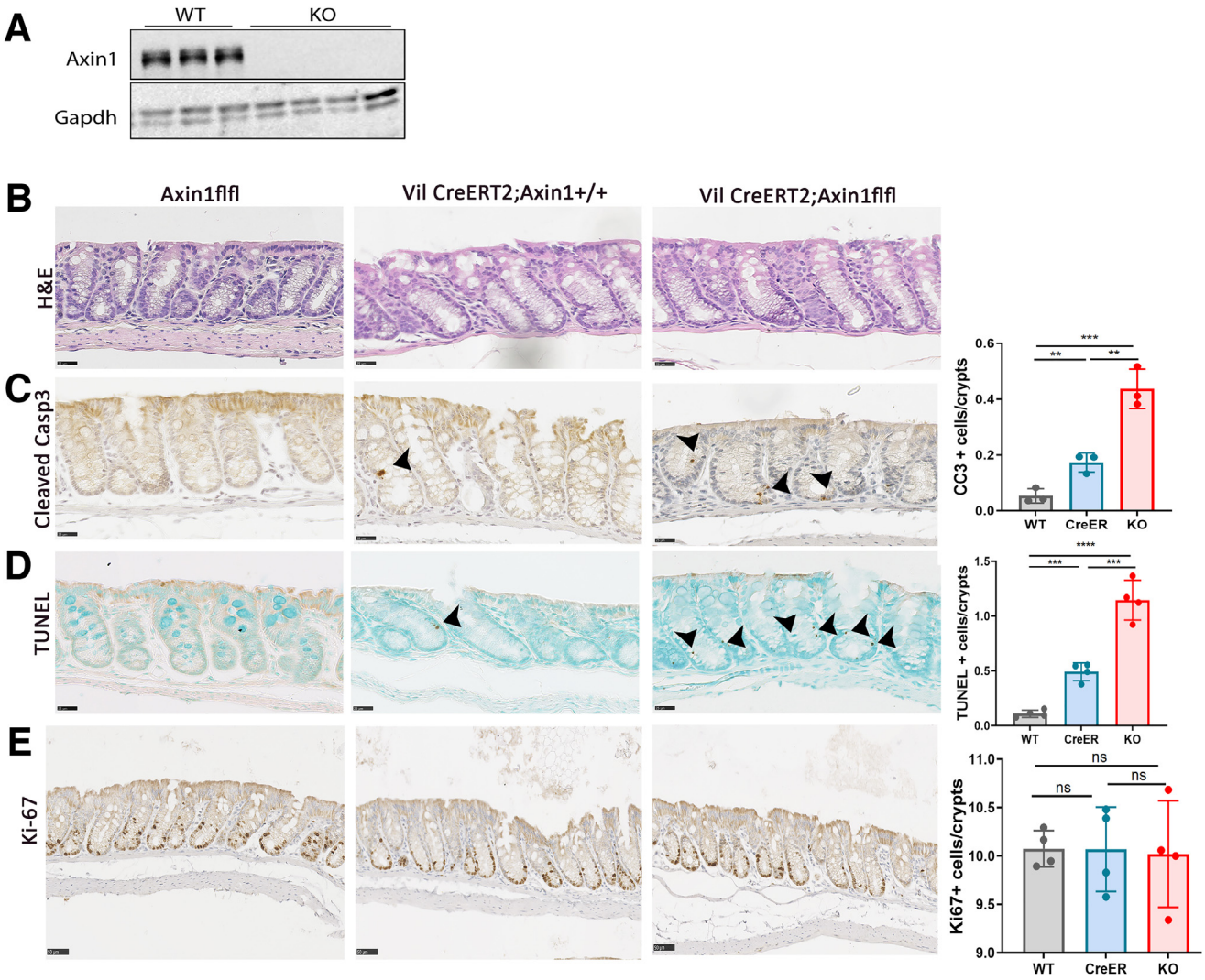

Figure 2. Acute deletion of *Axin1* in the mouse colon. (*A*) Western blot analysis of Axin1 and Gapdh on whole colon tissue lysates from WT (2 Axin1^{flfl} and 1 Vil CreER^{T2};Axin1$^{+/+}$) and 4 KO (Axin1$^{\Delta IEC}$) mice killed on day 5 postinduction. Gapdh served as a loading control. (*B–E*) Histologic analyses of the colon of WT (Axin1$^{fl/fl}$ and Vil CreER^{T2};Axin1$^{+/+}$) and KO (Axin1$^{\Delta IEC}$) mice. The mice were killed on day 5, after 4 days of tamoxifen injections. H&E staining of representative colon sections from WT (Axin1^{flfl} or Vil CreER^{T2};Axin1$^{+/+}$) and KO (Axin1$^{\Delta IEC}$) mice. *Scale bar for H&E*: 25 μm. Cleaved caspase 3 (*Scale bar*: 25 μm), TUNEL *(Scale bar*: 25 μm) , and Ki-67 staining of representative colonic epithelium sections from WT (Axin1$^{fl/fl}$ or Villin^{Cre+};Axin1$^{+/+}$) and KO (Axin1$^{\Delta IEC}$) mice. Hematoxylin and methyl green were used as a nuclear counterstain for cleaved caspase 3, Ki-67, and TUNEL staining, respectively. Determination of the combined mean number of cleaved caspase 3–positive cells, TUNEL-positive cells per crypt of more than 20 consecutive whole colonic crypts in 8 WT (4 Axin1$^{fl/fl}$, 4 Vil CreER^{T2};Axin1$^{+/+}$) and 4 KO (Axin1$^{\Delta IEC}$) mice. *Black arrowhead* are Cleaved Casp3 and TUNEL positive cells respectively. $^{**}P < .01$, $^{***}P < .001$, and $^{****}P < .0001$.

Figure 1. (***See previous page***). **Acute deletion of *Axin1* in the small intestine of mice.** (*A*) Western blot analysis of Axin1 and Gapdh in whole–small intestine tissue lysates from WT (2 Axin1$^{fl/fl}$ and 2 Vil CreER^{T2};Axin1$^{+/+}$) and KO (4 Axin1$^{\Delta IEC}$) mice. Gapdh served as a loading control. The mice were killed on day 5, after 4 days of tamoxifen injections. (*B–E*) Histologic analyses of WT (Axin1$^{fl/fl}$ and Vil CreER^{T2};Axin1$^{+/+}$) and KO (Axin1$^{\Delta IEC}$) mice. The mice were killed on day 5, after 4 days of tamoxifen injections. H&E staining of representative intestinal sections from WT and KO mice with apoptotic cells in KO mice highlighted by *black arrowheads*. *Scale bar for H&E*: 25 μm. Cleaved caspase 3, TUNEL, and Ki-67 staining of representative small intestine epithelium sections from WT and KO mice. Hematoxylin and methyl green were used as a nuclear counterstain for cleaved caspase 3 (*scale bar*: 25 μm), TUNEL staining (*scale bar*: 50 μm), and Ki-67 staining (*scale bar*: 50 μm). Determination of the mean number of cleaved caspase 3–positive cells and of TUNEL-positive cells per crypt was performed with a combined average of more than 40 consecutive whole crypts from 8 WT (4 Axin1$^{fl/fl}$, 4 Vil CreER^{T2}; Axin1$^{+/+}$) and 4 KO (Axin1$^{\Delta IEC}$) mice (N = 4 per group). (*F*) Transient apoptosis induced by Cre ER^{T2} activation. Experimental design. KO (Axin1$^{\Delta IEC}$) mice received 4 daily injections of tamoxifen and then were killed on day 5 or day 15. Representative TUNEL staining on small intestine sections from KO (Axin1$^{\Delta IEC}$) mice on days 5 and 15 after tamoxifen injection. Methyl green was used as a nuclear counterstain. *Scale bar*: 25 μm. Determination of the mean number of TUNEL-positive cells per crypt was performed with a combined average of more than 40 consecutive whole crypts from WT (Axin1$^{fl/fl}$) and KO (Axin1$^{\Delta IEC}$) mice (N = 4 per group). (*G*) Western blot analysis of Axin1 and Gapdh on whole intestine tissue lysates from WT (2 Axin1$^{fl/fl}$ and 1 Vil CreER^{T2};Axin1$^{+/+}$;Axin1$^{+/+}$) and 4 KO (Axin1$^{\Delta IEC}$) mice killed 15 days after induction. Gapdh served as a loading control. Significant differences as follows: $^{***}P < .001$, and $^{****}P < .0001$.

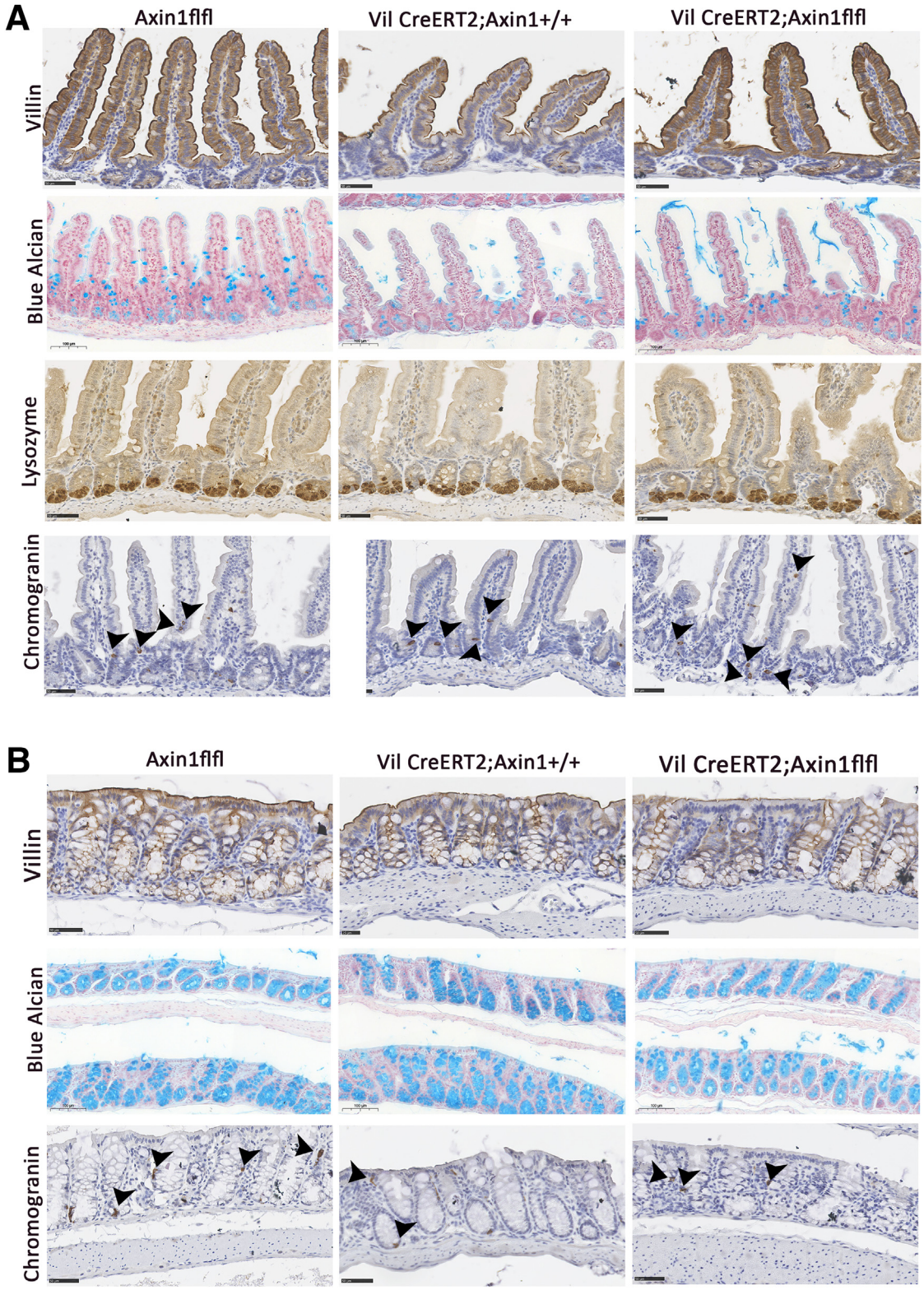

Figure 3. *Axin1* deficiency does not impair intestinal differentiation in mouse small intestine and colon. (*A*) Villin, Alcian blue, lysozyme, and chromogranin B staining of representative intestinal sections from WT ($Axin1^{fl/fl}$ or Vil $CreER^{T2}$;$Axin1^{+/+}$) and KO ($Axin1^{\Delta IEC}$) mice. The mice were killed on day 5, after 4 days of tamoxifen injections. Hematoxylin and fast red were used as a nuclear counterstain for villin, lysozyme, and chromogranin B staining (*scale bar*: 50 μm), and for Alcian blue staining (*scale bar*: 100 μm), respectively. *Scale bar*: 100 μm. (*B*) Villin, Alcian blue, and chromogranin B staining of representative colon sections from WT ($Axin1^{fl/fl}$ or Vil $CreER^{T2}$;$Axin1^{+/+}$) and KO ($Axin1^{\Delta IEC}$) mice. The mice were killed on day 5, after 4 days of tamoxifen injections. Hematoxylin and fast red were used as a nuclear counterstain for villin and chromogranin B staining (*scale bar*: 50 μm), and for Alcian blue staining (*scale bar*: 100 μm), respectively. *Black arrowheads* are chromogranin-positive cells.

Sp5 and *Sox9* in the colon is consistent with the regional-specific response of the Wnt/β-catenin signaling that showed activation of partially distinct sets of target genes in the intestine.[18] In agreement with our data, a constitutive Wnt activation in organoids of all parts of the intestine showed an increase of *Sox9* expression in the small intestine and no induction in the colon.[18] No induction of β-catenin target genes was observed in control mice or in mice with single deficiencies of *Axin1* or *Axin2* (Figure 7).

Thus, *Axin2* compensated for the loss of *Axin1* in the down-regulation of Wnt/β-catenin signaling. We performed additional analyses on the liver, in which we also previously had observed a lack of activation of Wnt/β-catenin signaling in mice with a targeted *Axin1* inactivation in hepatocytes.[9] This aspect was of particular interest because the domain in which *Axin1* and *Axin2* are co-expressed is smaller in the liver lobule than in the intestine, in which it covers the entire crypt, with a gradient from the bottom to the top. In the liver, *Axin1* and *Axin2* co-expression is restricted to a ring of 1 to 3 pericentral hepatocytes around the central vein, in which Wnt/β-catenin signaling is activated.[19] By injecting an adeno-associated virus encoding the Cre recombinase into $Axin1^{fl/fl}$ or ($Axin1^{fl/fl}$;$Axin2^{lacZ, lacZ}$) mice, resulting in the inactivation of *Axin1*, or of the combined deletion of *Axin1* and *Axin2*, respectively, in all hepatocytes within the liver, we observed that inactivation of *Axin1* in hepatocytes did not disturb metabolic zonation, as shown by the absence of change in expression of the pericentral marker *Glul*, a well-defined liver β-catenin target gene[20] (Figure 7*D*). This finding is consistent with our previously published results.[9] Similar results were obtained for the inactivation of *Axin2* in the hepatocytes of Axin2KO mice (Figure 7*D*). However, in the livers of mice with a combined inactivation of *Axin1* and *Axin2* in hepatocytes, we observed a complete disruption of metabolic zonation, with *Glul* expression throughout the entire liver lobule (Figure 7*D*). These results attest to the occurrence of Wnt/β-catenin activity throughout the livers of DKO mice, suggesting that there was sufficient *Axin2* expression outside the perivenous area to compensate for the loss of *Axin1*, despite the lack of activation of Wnt/β-catenin signaling. As in the intestine, we found that the combined loss of A*xin1* and *Axin2* in hepatocytes phenocopied *Apc* loss in the liver, both for the metabolic zonation and for the control of cell proliferation with a strong increase in cell proliferation shown by Ki-67 staining (Figure 7*D*). This is consistent with our previous work.[21]

These results indicate that *Axin2* can compensate for the loss of *Axin1* in the down-regulation of Wnt/β-catenin activity in multiple tissues.

Axin1 Protects Against the Development of Chemically Induced Colorectal Tumorigenesis

We characterized the tumor-suppressor function of Axin1 with the AOM/DSS protocol, which is widely used in studies of colitis-associated CRC.[22] $Axin1^{\Delta IEC}$ mice and their wild-type (WT) $Axin1^{fl/fl}$ littermates were treated with the carcinogen AOM and then with 3 cycles of 2.5% DSS in drinking water, separated by periods of normal drinking water. This treatment resulted in chronic inflammation that supported the growth of the neoplastic epithelium induced by AOM (Figure 8*A*). We assessed the colitis phenotype by monitoring changes in body weight. We found that *Axin1*-deficient mice lost significantly less weight than control mice at each cycle of DSS treatment, suggesting that *Axin1* loss in intestinal epithelial cells may protect against DSS-induced toxicity (Figure 8*B*). At the experimental end point, 100 days after the initial AOM injection, a macroscopic evaluation of the dissected and washed colon indicated that tumors had developed in both mutant and control mice, mostly in the distal colon (Figure 8*C*). $Axin1^{\Delta IEC}$ mice developed significantly more tumors than WT mice (Figure 8*D*). Further histologic analyses of the size of the tumors showed that $Axin1^{\Delta IEC}$ mice had significantly larger numbers of small tumors, suggesting that Axin1 influences tumor initiation (Figure 8*E*). All of the tumors were well-differentiated adenocarcinomas (Figure 8*F*). We also evaluated cell proliferation by Ki-67 staining of the tumors. There were larger numbers of Ki-67–positive cells in the tumors of $Axin1^{\Delta IEC}$ mice than in those of WT mice (Figure 8*G*). AOM is carcinogenic in rodent colonic epithelial cells through the induction of changes to the Wnt/β-catenin pathway, mostly through *Ctnnb1* mutations.[23] We investigated whether the higher cell proliferation level and larger numbers of tumors in $Axin1^{\Delta IEC}$ mice were associated with an increase in β-catenin activity resulting from *Axin1* deficiency. Immunohistochemical staining for β-catenin on $Axin1^{\Delta IEC}$ and WT tumors showed no increase in the overall cytosolic/nuclear β-catenin staining (Figure 8*H*). An analysis of the expression of several β-catenin target genes in tumors developed in $Axin1^{\Delta IEC}$ mice and in their WT counterparts confirmed the absence of an increase in β-catenin activity between tumors developed in $Axin1^{\Delta IEC}$ and WT mice (Figure 8*I*). As expected, from the presence of *Ctnnb1* mutation in AOM/DSS-induced colon tumors,[23] expression of the β-catenin target genes were induced in all the tumors (WT and KO) compared with the nontumoral tissue (Figure 8*I*). Collectively, these results showed that tumors that developed in the $Axin1^{\Delta IEC}$ mice did not display higher levels of β-catenin activity than those that developed in WT animals.

For confirmation of protection against DSS toxicity, we examined the response of $Axin1^{\Delta IEC}$ mice to acute treatment with DSS. $Axin1^{\Delta IEC}$ mice and their control $Axin1^{fl/fl}$ littermates were treated for 7 days with 3% DSS in drinking water, and then were allowed to recover on normal drinking water for 6 days. From day 5 of DSS treatment, the $Axin1^{\Delta IEC}$ mice lost significantly less weight than the controls. Furthermore, most of the KO mice presented weight recovery on day 13, whereas none of the WT mice had recovered their normal weight at this time point (Figure 9*A*). The WT mice had a shorter colon than the KO mice after DSS treatment (Figure 9*B*). These results confirm that epithelial *Axin1* deficiency leads to less severe colitis than was observed in WT mice after DSS treatment. Consistent with this less severe colitis, the histologic score, reflecting inflammation and epithelial damage, was significantly lower in $Axin1^{\Delta IEC}$ mice than in controls (Figure 9*C*). Surprisingly, as shown in Figure 9*D*, there was no significant difference between the

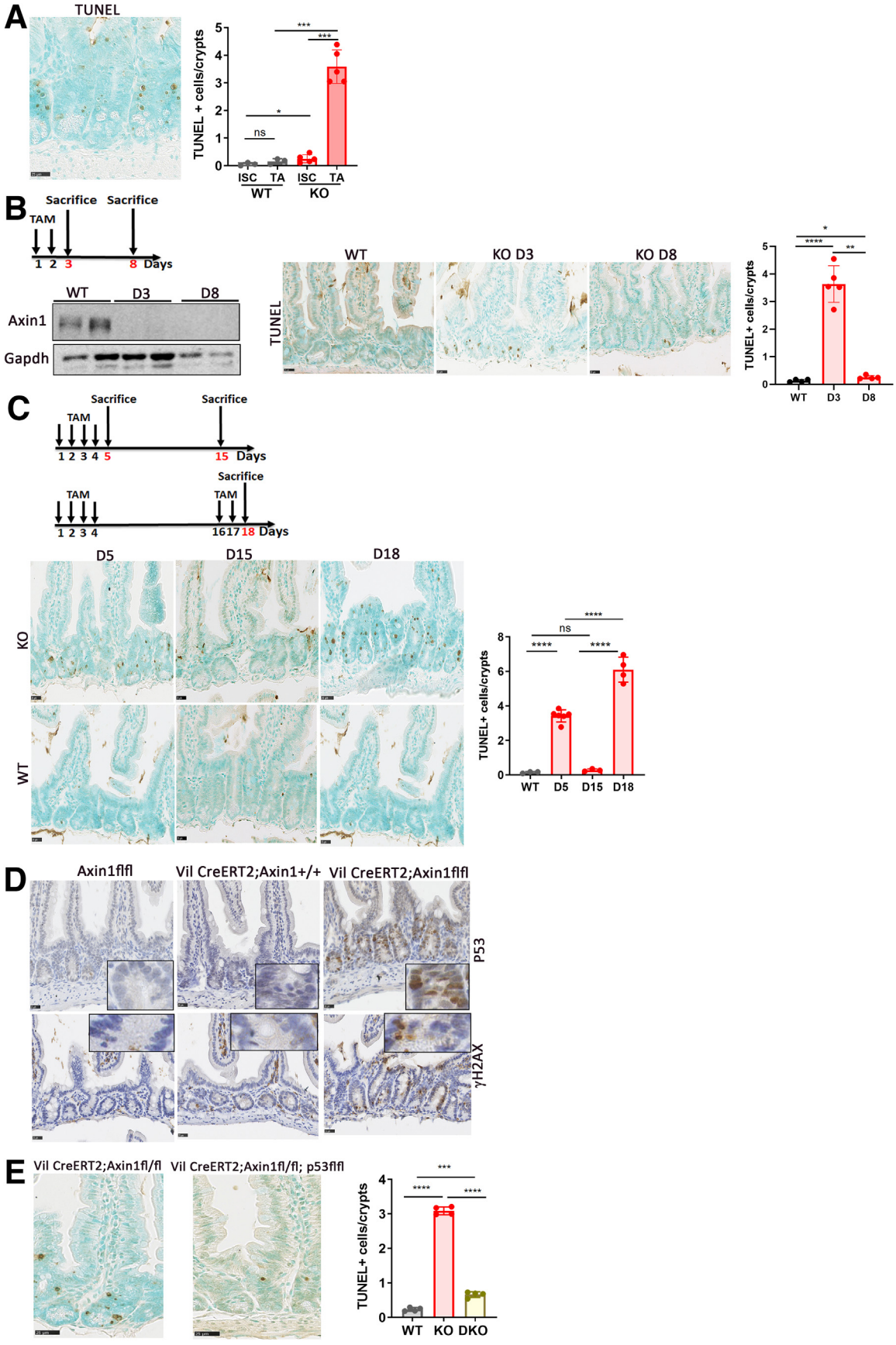
A
TUNEL
TUNEL + cells/crypts
ns
*
***
***
ISC TA ISC TA
WT KO
B
TAM
Sacrifice Sacrifice
1 2 3 8 Days
WT D3 D8
Axin1
Gapdh
WT KO D3 KO D8
TUNEL
TUNEL+ cells/crypts
*
****
**
WT D3 D8
C
TAM
Sacrifice Sacrifice
1 2 3 4 5 15 Days
TAM TAM
Sacrifice
1 2 3 4 16 17 18 Days
D5 D15 D18
KO
WT
TUNEL+ cells/crypts
****
ns
****
****
WT D5 D15 D18
D
Axin1fl/fl Vil CreERT2;Axin1+/+ Vil CreERT2;Axin1fl/fl
P53
γH2AX
E
Vil CreERT2;Axin1fl/fl Vil CreERT2;Axin1fl/fl; p53fl/fl
TUNEL+ cells/crypts
***
****
****
WT KO DKO

intestinal permeability, as measured by the tetramethylrhodamine B isothiocyanate (TRITC)-dextran assay, in the colon of Axin1$^{\Delta IEC}$ and WT mice that were challenged by DSS (Figure 9*D*).

Consistent with the colitis scores, the increase in messenger RNA levels for proinflammatory cytokines/chemokines (*Il6*, *Il1β*, *Tnfα*, *Cxcl10*, *Ccl2*) after DSS treatment was smaller in mutant mice than in controls (Figure 9*E*). The residual expression of *Axin1* in mutant mice may result from its expression in nonepithelial intestinal cells. Altogether, these results suggest that a protective mechanism operates in Axin1$^{\Delta IEC}$ mice, limiting gut inflammation after DSS treatment.

Collectively, these results show that Axin1 has a tumor-suppressor function in the intestine that does not appear to be linked to an increase in activation of the Wnt-β-catenin pathway. Axin1$^{\Delta IEC}$ mice were prone to the development of larger numbers of colorectal cancers upon AOM/DSS treatment, despite having a weaker colonic inflammatory response after acute DSS treatment.

Axin1 Controls an Immune IFNγ/Th1 Inflammatory Response

We investigated how Axin1 might be able to both stimulate an inflammatory response in the gut and to protect against tumorigenesis by comparing first the transcriptome profiling data for tumors developing in Axin1$^{\Delta IEC}$ and WT mice by RNA sequencing (RNA-seq) and then the transcriptome profiles of colon tissues from Axin1$^{\Delta IEC}$ and WT mice treated with DSS on day 7 and day 13 that was compared with those for untreated WT mice receiving drinking water.

RNA-seq analysis of the tumors from *Axin1*-deficient and WT mice identified 327 differentially expressed genes (DEGs) ($P < .05$; fold change, $>\pm 2$), 232 of which were down-regulated in the *Axin1*-deficient mice (Supplementary Table 1). Interestingly, functional annotation analysis with IPA (Quiagen) and ClueGo software identified the IFN signaling and immune Th1 pathways as the highest-ranking enriched pathways inhibited in the tumors of Axin1$^{\Delta IEC}$ mice (Figure 10*A*, and Table 3 in Figure 10). Consistent with these results, gene set enrichment analysis (GSEA) with the Hallmark gene sets identified IFNγ response, allograft rejection, inflammatory response, and tumor necrosis factor (TNF)α signaling via nuclear factor-κB (NF-κB) as significantly down-regulated in the tumors of Axin1$^{\Delta IEC}$ mice relative to those in WT mice (Figure 10*B*). In addition, GSEA with the Biocarta profile identified the interleukin (IL)12 pathway, a major pathway for the development of Th1-type immune responses against cancer,[24] as significantly down-regulated in the tumors of KO mice relative to their WT counterparts (Figure 10*C*). Consistent with these results, a heatmap of the immune Th1 signature showed this signature to be less strongly expressed in tumors from *Axin1*-mutant mice than in WT mice, and confirmed the decreased expression of Il12 (Figure 10*D*). Upstream regulator analysis with IPA software identified IFNγ/signal transducer and activator of transcription (STAT)1 among the top-ranking cytokine upstream regulators for which significant inhibition was predicted (Table 3 in Figure 10). Stat1 plays a vital role in IFNγ signaling and is essential for Th1 cell differentiation.[25] Collectively, these results suggest a down-regulation of the IFNγ/STAT1/Th1 immune response in the tumors of Axin1$^{\Delta IEC}$ mice. Interestingly, these pathways are known to play a major role in antitumor immunity,[26] and

Figure 4. (*See previous page*). Sensitivity of *Axin1*-deficient crypts to the toxicity induced by Cre ER^{T2} activation in the small intestine. (*A*) Apoptosis mostly affected progenitor cells in the crypt of the small intestine. Representative TUNEL staining of Axin1$^{\Delta IEC}$ mice on day 5 after tamoxifen injection, showing that most of the TUNEL-positive cells are located in the progenitor compartment of the crypt rather than in the intestinal stem cell (ISC) compartment of the crypt. Determination of the combined mean number of TUNEL-positive cells of more than 30 whole crypts in WT and KO mice in the progenitor compartment of the transit-amplifying (TA) cells and in the ISC compartment (N = 3 per group). The ISC and the TA compartment were defined relative to the Paneth cell zone by considering the TA cells as the cells of the crypts located above the Paneth cells. (*B*) Transient apoptosis induced by Cre ER^{T2} activation. Experimental design. WT (Axin1^{flfl}) and KO (Axin1$^{\Delta IEC}$) mice received 2 daily doses of tamoxifen by injection and were killed on day 3 or day 8. Western blot of Axin1 and Gapdh on whole-intestine tissue lysates from WT and KO mice on days 3 and 8. Gapdh served as a loading control. Representative TUNEL staining on small intestine sections from WT and KO mice on days 3 and 8. Methyl green was used as a nuclear counterstain. Determination of the combined mean number of TUNEL-positive cells per crypt of more than 40 consecutive whole crypts in WT and KO mice on days 3 and 8 (N= 3 per group). *Scale bar*: 25 μm. (*C*) Effect of a new tamoxifen treatment. Experimental design. The first group of mice received 4 daily doses of tamoxifen and were killed on day 5 or 15. The second group of mice underwent the same protocol and received 4 daily doses of tamoxifen, however, on day 15, they received 2 new doses of tamoxifen before being killed on day 18. Representative TUNEL staining on small intestine sections from WT (Axin1$^{fl/fl}$) and KO (Axin1$^{\Delta IEC}$) mice on days 5, 15, and 18. Methyl green was used as a nuclear counterstain. Determination of the combined mean number of the TUNEL-positive cells per crypt of more than 40 consecutive whole crypts in WT and KO mice on days 5, 15, and 18 (N = 3 per group). *Scale bar*: 25 μm. (*D*) Representative p53 and γ H2ax staining on intestinal epithelium sections from WT (Axin1$^{fl/fl}$ and Vil CreER^{T2};Axin1$^{+/+}$) and KO (Axin1$^{\Delta IEC}$) mice on day 5, after 4 daily doses of tamoxifen. Hematoxylin was used as a nuclear counterstain. *Scale bar*: 25 μm. (*E*) Absence of apoptosis in crypts with a combined deficiency of both Axin1 and p53. Representative TUNEL staining on intestinal sections from Axin1-deficient (Axin1$^{\Delta IEC}$) mice and mice with combined Axin1/p53 deficiency (Vil CreER^{T2};Axin1$^{fl/fl}$;p53$^{fl/fl}$) on day 5. Methyl green was used as a nuclear counterstain. Determination of the combined mean number of TUNEL-positive cells per crypt of more than 40 consecutive whole crypts in WT (Axin1$^{fl/fl}$); Axin1$^{\Delta IEC}$(Vil CreER^{T2};Axin1$^{fl/fl}$); Axin1, p53$^{\Delta IEC}$(Vil CreER^{T2};Axin1$^{fl/fl}$;p53$^{fl/fl}$) mice (N= 3 per group). *Scale bar*: 25 μm. Significant differences as follows: *$P < .05$, **$P < .01$, ***$P < .001$, and ****$P < .0001$.

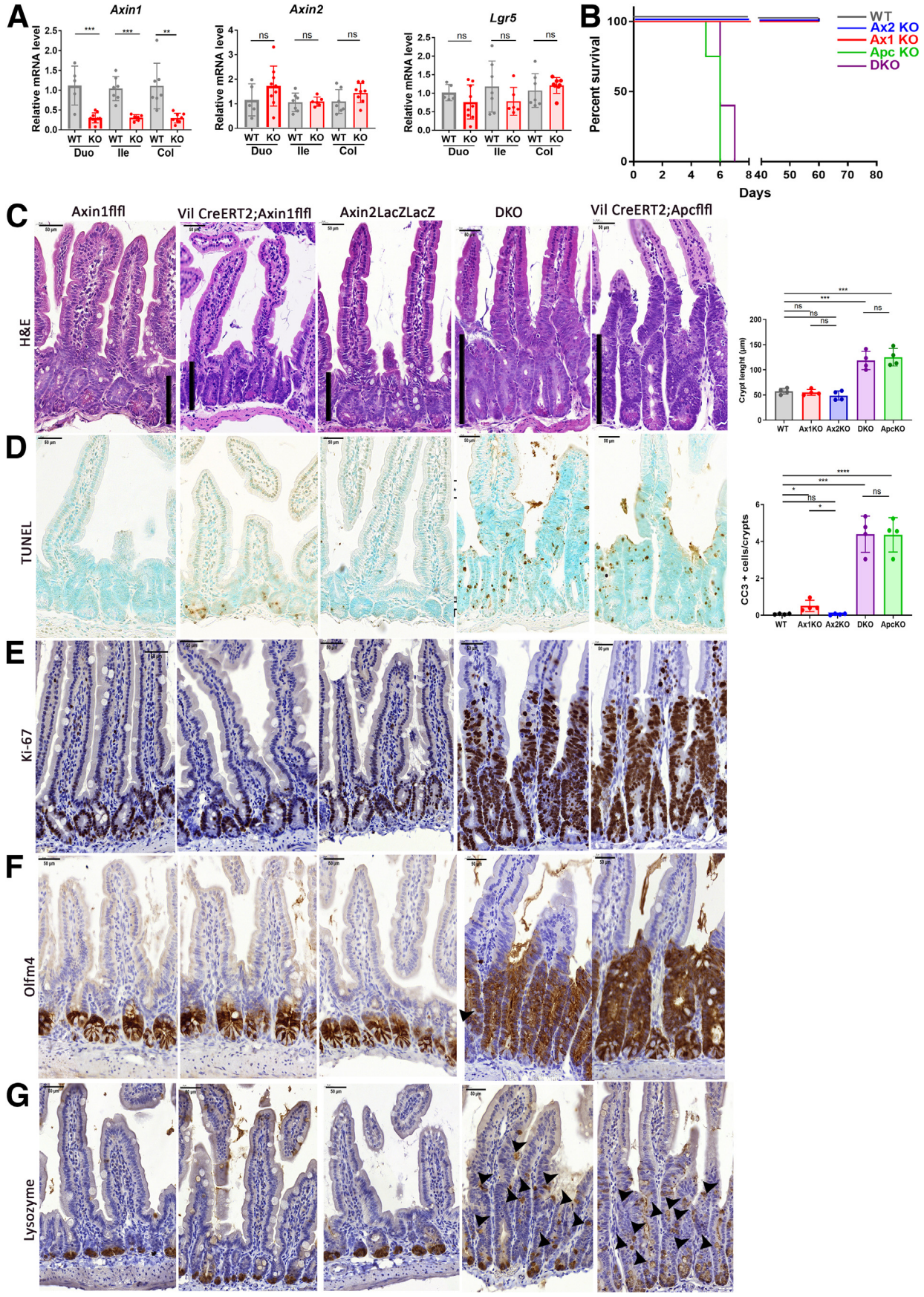
A
Axin1
Axin2
Lgr5
Relative mRNA level
WT KO WT KO WT KO
Duo Ile Col
B
Percent survival
Days
WT
Ax2 KO
Ax1 KO
Apc KO
DKO
C
Axin1flfl
Vil CreERT2;Axin1flfl
Axin2LacZLacZ
DKO
Vil CreERT2;Apcflfl
H&E
Crypt lenght (µm)
WT Ax1KO Ax2KO DKO ApcKO
D
TUNEL
CC3 + cells/crypts
E
Ki-67
F
Olfm4
G
Lysozyme

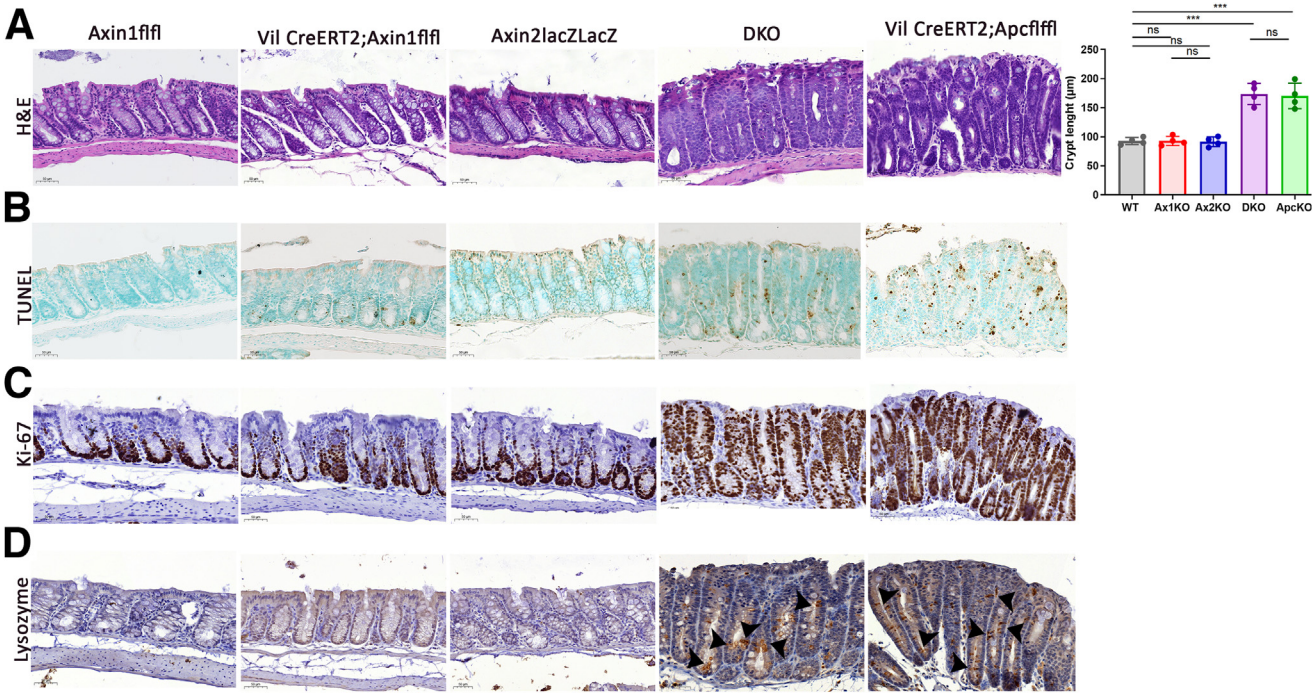

Figure 6. Mice with combined deficiencies of *Axin1* and *Axin2* in the colon are phenocopies of *Apc*-deficient mice. (*A*) Representative H&E staining of colon sections from WT (Axin1$^{fl/fl}$), KO (Axin1$^{\Delta IEC}$), Axin2KO, DKO and Apc$^{\Delta IEC}$ mice. Determination of mean crypt length (N = 4 per group). (*B–D*) Representative TUNEL, Ki-67, and lysozyme staining on colon sections from WT (Axin1$^{fl/fl}$), KO (Axin1$^{\Delta IEC}$), Axin2KO, DKO, and Apc$^{\Delta IEC}$ mice. Hematoxylin and methyl green were used as a nuclear counterstain for Ki-67, lysozyme, and TUNEL staining, respectively. *Scale bars*: 50 μm. The mice were killed on day 5, after 4 days of tamoxifen injections.

specifically in CRC.[27] To support a decrease in the Th1-mediated immunosurveillance in the tumors of Axin1$^{\Delta IEC}$ mice, we quantified by immunohistochemistry the infiltration of the lymphocytes T CD8^{+} in the tumors. As expected, a significant decrease in the number of CD8^{+} T cells was observed in tumors of Axin1$^{\Delta IEC}$ mice compared with tumors that developed in their WT counterparts (Figure 10*F*). We also identified 4 gene sets that were up-regulated significantly in the tumors of KO mice relative to those of WT mice. These gene sets included genes encoding adenoviral early region 2 binding factor targets, G2M checkpoint, and mitotic spindle proteins. These data are consistent with the increase in Ki-67 staining we described in Figure 8*G*.

We then analyzed the colon transcriptional profile of KO and WT mice treated with DSS on day 7 and day 13 (Supplementary Table 2). As expected, GSEA identified major pathways of gut inflammation enriched in the colon of WT mice treated with DSS on day 7 and day 13, respectively, that were compared with untreated WT animals (Figure 11*A*). We then used GSEA analysis to compare the transcriptome profiles of Axin1$^{\Delta IEC}$ mice treated with DSS on day 7 and day 13, respectively, with their WT counterparts. Strikingly, we observed opposite patterns of change in the expression of the gut inflammatory gene sets, for which the WT DSS-treated group showed positive enrichment relative to the untreated WT group, whereas the *Axin1*-mutant DSS-treated group showed negative enrichment relative to the WT DSS-treated group (Figure 11*A*). Therefore, there was a significant down-regulation of gut inflammatory pathways in *Axin1*-deficient mice after treatment with a single dose of DSS on both day 7 and day 13 (Figure 11*A*). Interestingly,

Figure 5. (*See previous page*). Mice with a combined deficiency of *Axin1* and *Axin2* in the small intestine phenocopy *Apc*-deficient mice. (*A*) Relative messenger RNA (mRNA) levels for *Axin1*, *Axin2*, and *Lgr5*, assessed by qRT-PCR analyses on the duodenum (Duo), ileum (Ile), and colon (Col) of WT (Axin1$^{fl/fl}$) and KO (Axin1$^{\Delta IEC}$) mice (N = 5 per group). (*B*) Kaplan–Meier survival curves for WT (Axin1$^{fl/fl}$, $n = 4$, gray), KO (Axin1$^{\Delta IEC}$, $n = 4$, blue), Axin2KO ($n = 4$, red), Apc$^{\Delta IEC}$ ($n = 3$, green), and DKO ($n = 4$, purple) mice. (*C–G*) H&E staining of representative small intestine sections from WT (Axin1$^{fl/fl}$), KO (Axin1$^{\Delta IEC}$), Axin2KO, DKO, and Apc$^{\Delta IEC}$ mice. *Scale bar*: 50 μm. Determination of mean crypt length (N = 4 per group). TUNEL, Ki-67, Olfm4, and lysozyme staining of representative small intestine epithelium sections from WT (Axin1$^{fl/fl}$), KO (Axin1$^{\Delta IEC}$), Axin2KO, DKO, and Apc$^{\Delta IEC}$ mice. Hematoxylin and methyl green were used as a nuclear counterstain for Ki-67, Olfm4, lysozyme, and TUNEL staining. *Scale bar*: 50 μm. Determination of the mean number of TUNEL-positive cells per crypt of more than 40 consecutive whole crypts in WT Axin1$^{fl/fl}$, KO (Axin1$^{\Delta IEC}$), Axin2KO, DKO, and Apc$^{\Delta IEC}$ mice (N = 3 per group). Mislocalization of lysozyme-positive cells in the enlarged crypts, highlighted by *black arrowheads*. The mice were killed on day 5, after 4 days of tamoxifen injections. Significant differences as follows: *$P < .05$, **$P < .01$, and ***$P < .001$.

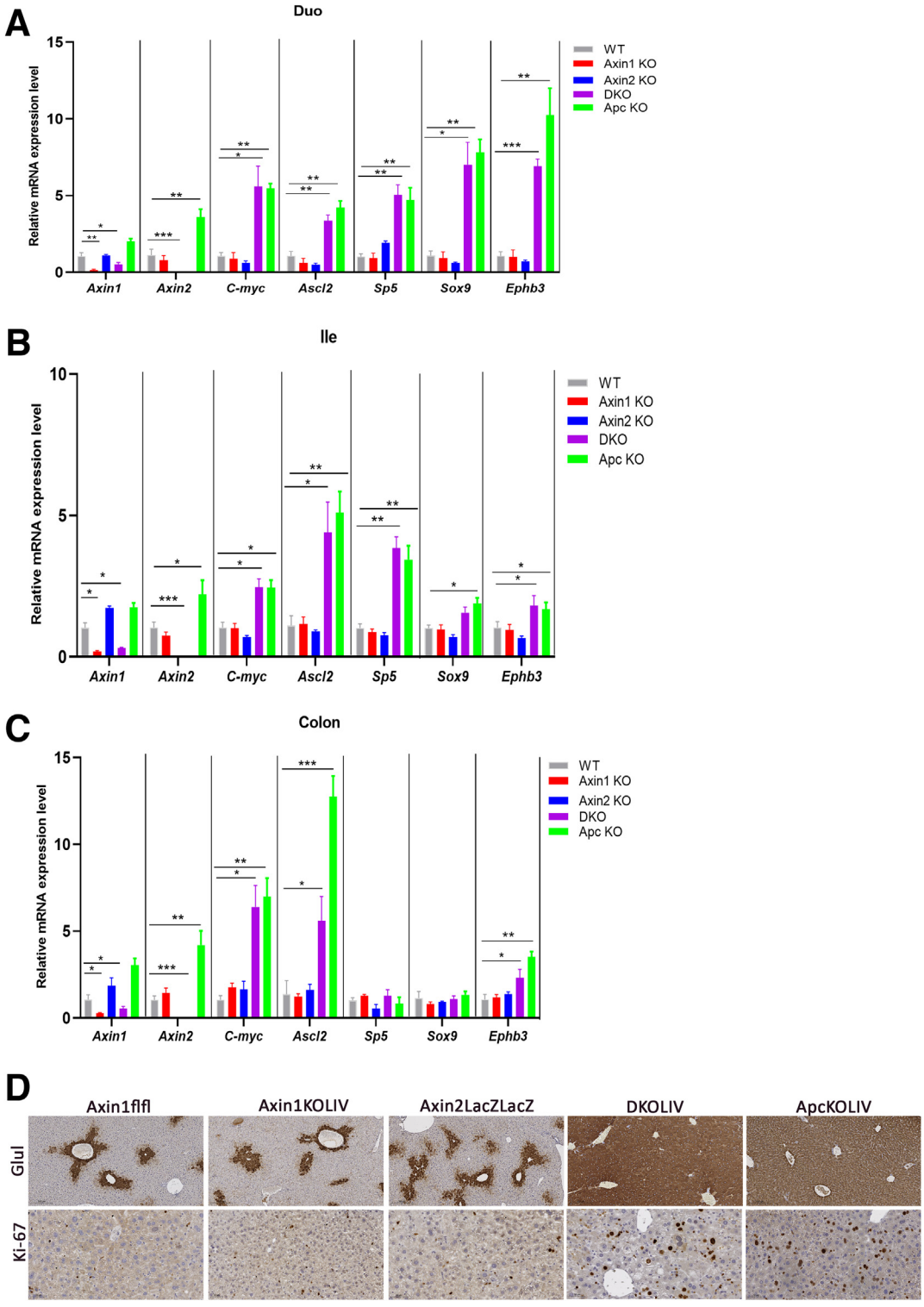

Figure 7. Activation of the Wnt/β-catenin pathway in the intestine and liver of mice with combined deficiencies of *Axin1* and *Axin2*. (*A*) Relative messenger RNA (mRNA) levels for *Axin1*, *Axin2*, *Ascl2*, *Sp5*, *Sox9*, and *Ephb3* assessed by qRT-PCR analysis on intestinal epithelium sections from the (*A*) duodenum, (*B*) ileum, and (*C*) colon of WT ($Axin1^{fl/fl}$, $n = 3$), KO ($Axin1^{\Delta IEC}$, $n = 4$), Axin2KO ($n = 3$), DKO ($n = 4$), and $Apc^{\Delta IEC}$ ($n = 4$) mice. The mice were killed on day 5, after 4 days of tamoxifen injections. (*B*) Glul and Ki-67 staining in the livers of WT ($Axin1^{fl/fl}$), Axin1KOLIV ($Axin1^{fl/fl}$ injected with Ad Cre), Axin2KO ($Axin2^{LacZLacZ}$), DKOLIV ($Axin1^{fl/fl}$;$Axin2^{LacZLacZ}$ injected with Ad Cre), and ApcKOLIV ($Apc^{fl/fl}$ injected with Ad Cre) mice. *Scale bars*: 200 μm (*top row*) and 50 μm (*bottom row*). Mice were killed 2 weeks after recombined adenovirus injection.

it was the same gut inflammatory pathways that were down-regulated in the tumors of mutant mice, including the IFNγ response, allograft rejection, inflammatory response, and TNF signaling via NF-κB (Figure 10*B*). These data are consistent with the qRT-PCR data presented in Figure 9*D* that showed a significant decrease of several proinflammatory cytokines and chemokines in colon of DSS-treated Axin1$^{\Delta IEC}$ mice vs their WT counterparts. Overall, these data indicate that *Axin1* loss in the colon attenuates gut inflammatory pathways, including IFNγ and TNF signaling.

For further identification of the pathways inhibited in the colon of Axin1$^{\Delta IEC}$ mice relative to WT controls after DSS treatment, we identified the DEGs commonly up-regulated in the WT DSS-treated group relative to the untreated WT group ($P < .05$; fold-change, ≥2) and down-regulated in the mutant DSS-treated group relative to the WT DSS-treated group ($P < .05$; fold change, ≥-2), on both day 7 and day 13 (Supplementary Table 3, Figure 11*B*). IPA and ClueGO analyses of these 385 DEGs identified inflammation and the immune Th1 pathway as the most significantly enriched pathways in KO DSS-treated mice (Figure 11*C* and Table 4 in Figure 11). Upstream regulator analysis identified IFNγ/STAT1 and NF-κB among the top-ranking upstream regulators showing significant down-regulation in KO DSS-treated mice (Table 5 in Figure 11). We then assessed the lymphocyte infiltration in Axin1$^{\Delta IEC}$ mice and controls upon DSS challenge using flow cytometry analysis. Lymphocytes were isolated from the lamina propria of colon of DSS-treated Axin1$^{\Delta IEC}$ and control mice and characterized for expression of different markers that define the Th1, Th17, and regulatory T-cell subsets. Consistent with the RNA-seq data, a significant decrease in the number of CD4$^+$TCRβ$^+$IFNγ$^+$ (Th1) cells was observed in the colonic lamina propria of Axin1$^{\Delta IEC}$ mice that was associated with a significant decrease in Th17 cells, while the regulatory T-cell population showed a similar number of cells in KO and WT mice (Figure 11*D*).

Altogether, these results identified epithelial Axin1 as a proinflammatory factor acting by promoting the development of an IFNγ/Th1 immune response in the colon. Interestingly, this inflammatory response is known to have antitumor immune activity and likely explain the tumor-suppressor function of Axin1 in the colonic mucosa.

The Gene Expression Signature From Axin1-*Deficient Mice Identifies CRC Patients With Poor Antitumor Immune Responses and Clinical Outcomes*

We then investigated whether the *Axin1*-dependent 327-GES defined by subjecting Axin1$^{\Delta IEC}$ and WT mice to the AOM/DSS protocol (Supplementary Table 1) was clinically and biologically relevant in patients with CRC. Our hypothesis was that if the Axin1 pathway indeed promotes the development of an appropriate IFNγ/Th1 antitumor response, *Axin1*-proficient tumors should be enriched in CRC patients from the consensus molecular subtype (CMS)1 (immune molecular subtype). We therefore applied the 327-gene signature to a transcriptomic database including 2239 primary clinical samples of CRCs (Table 1). Samples were classified either in the *Axin1*-proficient-like group (N = 1053), for those enriched with genes up-regulated in the WT mice, or in the *Axin1*-deficient-like group (N = 1186), for those enriched with genes up-regulated in the Axin1$^{\Delta IEC}$ mice. Clinical, pathologic, and molecular variables then were compared between the 2 groups.

Relative to Axin1-proficient-like tumors, Axin1-deficient-like tumors were enriched (Fisher exact test) in distal colon tumors from male patients, frequently stage 4, mismatch repair-proficient (pMMR) and of CMS2 subtype that is associated with Wnt activation (Table 2). As hypothesized, the Axin1-proficient-like tumors were enriched in the CMS1 subtype relative to Axin1-deficient-like tumors (30% vs 9%) (Table 2), and, to a lesser extent, enriched in the CMS4 subtype (34% vs 27%) (Table 2).

Disease-free survival (DFS) data were available for 1843 patients who had undergone surgery for primary CRC. The median follow-up period was 43 months (range, 1–212 mo); 120 patients (20%) had experienced an event, and the 5-year DFS was 66% (95% CI, 33–68) (Figure 12*A*). The 5-year DFS was lower in the Axin1-deficient-like group (63%; 95% CI, 60%–67%) than in the Axin1-proficient-like group (68%; 95% CI, 65%–72%; $P = 1.69E-02$, log-rank test) (Figure 12*B*). In univariate analysis (Figure 12*C*, Wald test), pathologic extension stage ($P = 1.48E-14$), MMR status ($P = 2.67E-03$), CMS ($P = 1.08E-03$), and the Axin1 GES signature-based group ($P = 1.71E-02$) were associated with DFS. In multivariate analysis (Figure 12*C*, Wald test), extension stage, MMR status, and the Axin1 GES signature-based group remained significant, suggesting that these variables were of independent prognostic value, whereas CMS tended toward significance.

We then compared several molecular variables, notably variables relating to immune landscape composition, between the Axin1-deficient-like and Axin1-proficient-like groups (Figure 12*D*). In silico analysis with the 24 immune cell types defined as the immunome[28] showed much lower levels of immune infiltrate (T cells, B cells, dendritic cells, macrophages, neutrophils, and so forth), and, more specifically, smaller cytotoxic cell subsets (CD8, Th1, cytotoxic, and γδ T cells) in the Axin1-deficient-like samples. Other immune functional signatures supported these observations: an impaired T-cell–inflamed signature,[29] low immunologic constant of rejection score[30] and immune cytolytic activity scores[31] for both innate and adaptive immune effector cells. This finding also is consistent with a profound defect of activation of the IFNα, IFNγ, and TNFα pathways,[32] antigen processing/presentation machinery score,[33] and a low score for the tertiary lymphoid structures signature.[34] These data showed that Axin1-deficient-like tumors from CRC patients have a profound defect of the Th1/IFNγ/cytotoxic antitumor response. This result obtained from the whole series also was confirmed in each molecular subtype (data not shown). Finally, the *Axin1*-deficient-like tumors also showed an enhanced activation of the transforming growth factor-β and lactic acidosis pathways, which are major inhibitors of the cytotoxic activity.

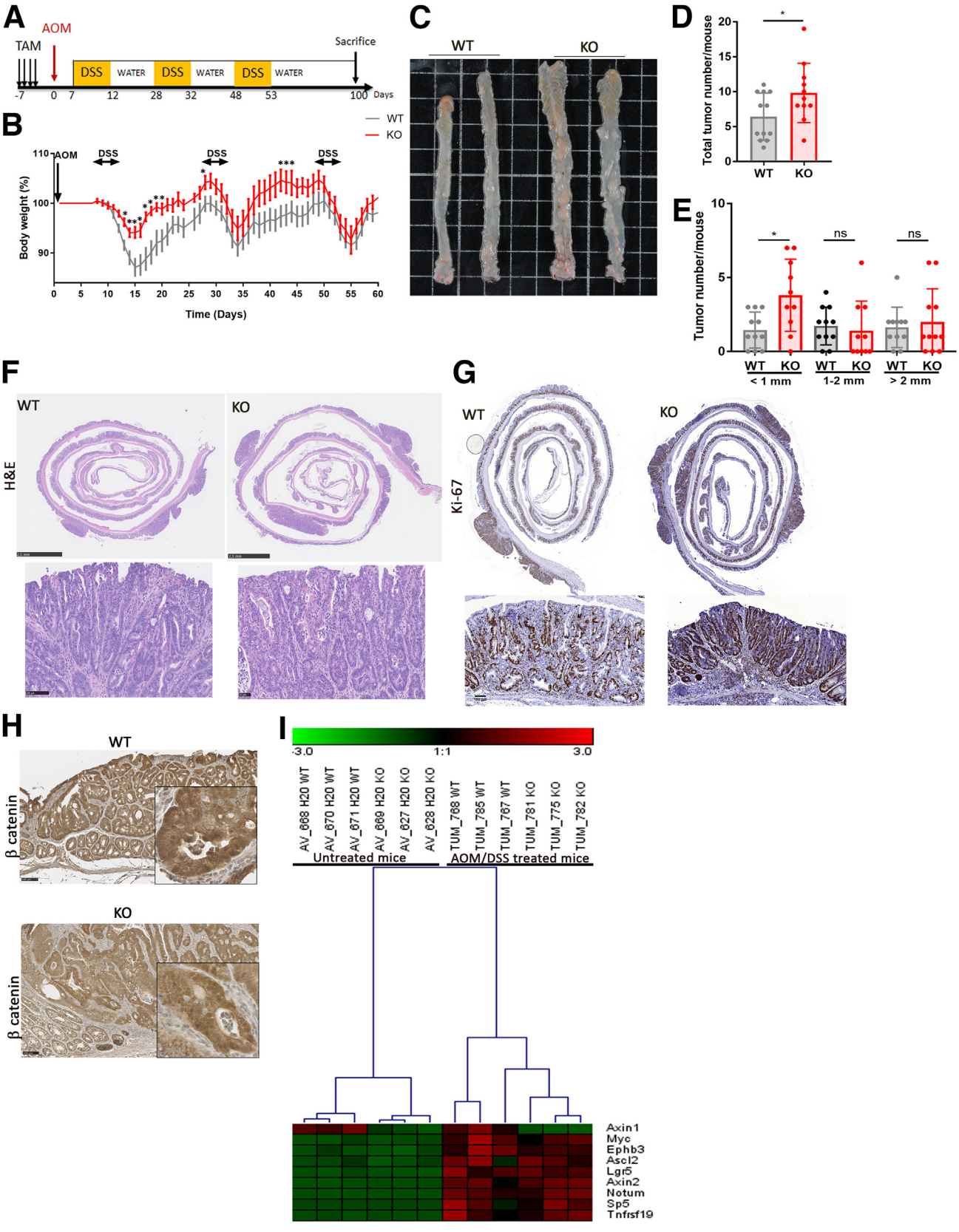
A
AOM
TAM
Sacrifice
DSS
WATER
DSS
WATER
DSS
WATER
-7
0
7
12
28
32
48
53
100
Days
B
WT
KO
AOM
DSS
DSS
DSS
Body weight (%)
110
100
90
0
5
10
15
20
25
30
35
40
45
50
55
60
Time (Days)
C
WT
KO
D
Total tumor number/mouse
20
15
10
5
0
WT
KO
E
Tumor number/mouse
10
5
0
ns
ns
WT
KO
WT
KO
WT
KO
< 1 mm
1-2 mm
> 2 mm
F
H&E
WT
KO
G
Ki-67
WT
KO
H
WT
β catenin
KO
β catenin
I
3.0
1:1
3.0
AV_668 H20 WT
AV_670 H20 WT
AV_671 H20 WT
AV_669 H20 KO
AV_627 H20 KO
AV_628 H20 KO
TUM_768 WT
TUM_785 WT
TUM_767 WT
TUM_781 KO
TUM_775 KO
TUM_782 KO
Untreated mice
AOM/DSS treated mice
Axin1
Myc
Ephb3
Ascl2
Lgr5
Axin2
Notum
Sp5
Tnfrsf19

These data highlight the clinical pertinence of our data from *Axin1*-deficient mouse models. Patients bearing CRCs with weak expression of the *Axin1*-dependent signature had a worse prognosis, associated with a significant decrease in the level of the immune antitumor response. Axin1 therefore appears to be an interesting new modulable target related to the antitumor immune response and clinical outcome.

Discussion

We show that *Axin1* is redundant with *Axin2* for down-regulation of Wnt/β-catenin signaling in the intestinal epithelium. *Axin1* is dispensable for intestinal homeostasis, deficiency of both *Axin1* and *Axin2* in the intestinal epithelium is required to phenocopy intestine-specific *Apc* knockout mice. This might explain why the Wnt/β-catenin pathway does not appear to be involved in the tumor-suppressor role of Axin1 in the intestine. We identify an unrecognized role for Axin1 in the control of the immune response in the intestine capable of accounting for its tumor-suppressor function. We found that *Axin1* deficiency in intestinal epithelial cells rendered mice more susceptible to chemically induced colon carcinogenesis, but reduced DSS-induced colitis by attenuating the induction of a proinflammatory program. RNA-seq analyses identified an IFNγ/Th1 immune program controlled by Axin1 that enhances the inflammatory response and protects against CRC. These observations in mice were complemented by in silico analysis of 2239 human CRC tumors, which showed that patients with weak expression of the *Axin1*-dependent GES had a worse prognosis and suggested that those with strong expression of the *Axin1*-dependent GES might benefit from immune checkpoint blockade.

We investigated the role of Axin1 in the intestine because of the crucial role of the Wnt pathway in the control of homeostasis and tumorigenesis of the gastrointestinal tract.[35] We found that *Axin1* was dispensable for normal intestinal homeostasis, its loss being compensated by *Axin2*. Mice with double *Axin1*, *Axin2* deficiencies in the intestinal epithelium phenocopied $Apc^{\Delta IEC}$ mice and died rapidly. The reason for the lethality likely is owing to the failed differentiation of the intestinal lineages induced by the aberrant Wnt activation that should alter the function of the intestine.[17,36] We expected the compensation of *Axin1* loss by *Axin2* for Wnt pathway down-regulation to be observed only in tissues in which Wnt signaling was activated because *Axin2* is a canonical β-catenin target gene.[37] We therefore analyzed the combined inactivation of *Axin1* and *Axin2* in the liver, in which the activation of Wnt signaling is restricted to a ring of a few hepatocytes around the central vein constituting the perivenous region of the liver lobule.[19] The Wnt pathway is not activated in most hepatocytes, and it is even inhibited in the periportal area owing to high levels of *Apc* expression.[19] We previously described the specific deletion of *Axin1* from all hepatocytes.[9] As reported here for intestinal cells, no particular phenotype was detected in the corresponding mice. Surprisingly, the combined deletion of *Axin1* and *Axin2* in hepatocytes led to an aberrant activation of β-catenin signaling throughout the liver lobule, even in the periportal area in which *Axin2* expression was not detected.[19] The liver phenotype of these mice mimicked that observed after targeted *Apc* loss in hepatocytes.[19] These results therefore suggest that the compensation of A*xin1* loss by A*xin2* also occurs in tissues in which Wnt/β-catenin signaling is not activated and in which *Axin2* expression levels are thought to be very low, such as periportal liver tissues. This surprising result supports the computational model of Lee et al,[38] who considered Axin1 to be rate-limiting for the destruction complex owing to its low levels.

We identified a new role for epithelial Axin1 in controlling gut inflammation that might be associated with its tumor-suppressor function. RNA-seq analyses of the colon of DSS-treated $Axin1^{\Delta IEC}$ and WT mice identified an IFNγ/Th1 proinflammatory program that was down-regulated in $Axin1^{\Delta IEC}$ mice. Flow cytometry analyses confirmed the reduction of the Th1 and Th17 cells in the lamina propria of DSS-treated $Axin1^{\Delta IEC}$ mice that corroborated the resistance of these mice to DDS-induced colitis. Thus, epithelial Axin1 appears to promote a proinflammatory response mediated by activation of the IFNγ/Th1 pathway. Interestingly, the same program also was found to be down-regulated in tumors developing in $Axin1^{\Delta IEC}$ mice after the AOM/DSS protocol. The IFNγ/Th1 pathway is known to have tumor-suppressor functions responsible for tumor clearance in several cancers, including CRC,[27,39,40] which could explain the increased AOM–DSS–driven colon tumorigenesis in $Axin1^{\Delta IEC}$ mice. Consistent with a decrease in immune surveillance, we detected by immunohistochemistry a decrease in the infiltration of the cytotoxic lymphocytes $CD8^{+}$ in tumors that developed in $Axin1^{\Delta IEC}$ mice. This correlates with the significantly large numbers of small tumors in the $Axin1^{\Delta IEC}$ mice and suggests that epithelial Axin1 suppresses the initiation of tumorigenesis. The tumor-suppressor function of Axin1 in the intestinal epithelial cells also involved a negative control of cell proliferation as shown by the strong increase in Ki-67 staining in tumors of $Axin1^{\Delta IEC}$ mice. Interestingly, the increase in cell

Figure 8. (*See previous page*). *Axin1* deficiency promotes the development of colon tumors. (*A*) Experimental protocol for AOM/DSS treatment. (*B*) Body weight changes during the AOM/DSS treatment of WT $Axin1^{fl/fl}$ ($n = 13$) and KO ($Axin1^{\Delta IEC}$, $n = 10$) mice. (*C*) Representative image of colons from WT and KO mice on day 100 after AOM treatment. (*D* and *E*) Tumor distribution in the colon of WT and KO mice on day 100 after AOM treatment. (*F*) H&E staining of representative sections of colon tumors from WT and KO mice on day 100 after AOM treatment, with a magnified *inset* in the lower row. *Scale bar*: 2.5 mm. (*G*) Ki-67 staining of representative sections of colon from WT and KO mice on day 100 after AOM treatment, with a magnified *inset* in the lower row. (*H*) Representative immunostaining for β-catenin of colon tumors from KO and WT mice, with a magnified *inset* in the lower row. *Scale bar*: 100 μm. (*I*) Heatmap indicating the expression of several β-catenin target genes in colon tumors from KO and WT mice and in the colon of untreated KO and WT mice. TAM, Tamoxifen.

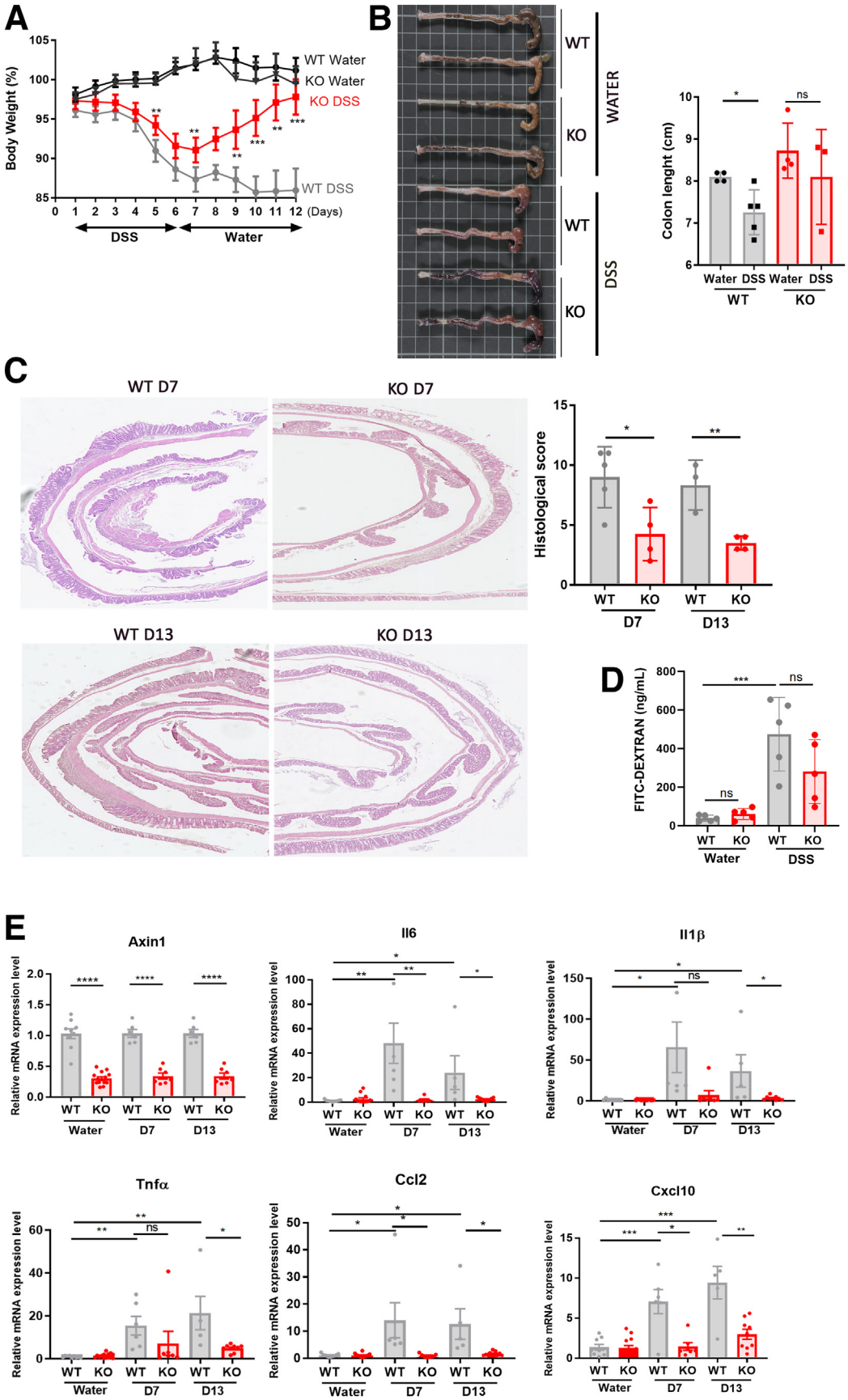
A
Body Weight (%)
WT Water
KO Water
KO DSS
WT DSS
(Days)
DSS
Water
B
WT
KO
WATER
WT
KO
DSS
Colon lenght (cm)
Water DSS Water DSS
WT
KO
C
WT D7
KO D7
WT D13
KO D13
Histological score
WT KO WT KO
D7
D13
D
FITC-DEXTRAN (ng/mL)
ns
WT KO WT KO
Water
DSS
E
Axin1
Il6
Il1β
Tnfα
Ccl2
Cxcl10
Relative mRNA expression level
WT KO WT KO WT KO
Water
D7
D13

proliferation in the tumors of Axin1$^{\Delta IEC}$ mice was not associated with an increase in Wnt/β-catenin signaling, likely owing to compensation by its paralog *Axin2*, induced in the tumors (Figure 8*I*).

The precise mechanism by which intestinal epithelial Axin1 exerts its tumor-suppressor function needs further clarification. Our data showed that Axin1$^{\Delta IEC}$ mice were more susceptible to AOM–DSS–driven colon tumorigenesis, but were more resistant to DSS-induced colitis. These observations are inconsistent with the paradigm that linked inflammation and cancer.[41] However, inflammation has the role of a double-edged sword in cancer and may either induce antitumor immunity or promote tumor development, specifically in CRC.[40] Indeed, in human beings, an IFNγ/Th1 response is characteristic of cancer immune surveillance, associated with Th1CD4^{+} and CD8^{+}T cells, which directly regulate tumor cell cytotoxicity and induce tumor suppression.[25] Our data strongly suggest that intestinal epithelial Axin1 exerts its tumor-suppressor function by inducing an antitumorigenic IFNγ/Th1 response. How epithelial Axin1 promotes a proinflammatory IFNγ/Th1 response remains to be investigated. We examined if it was via an epithelium-extrinsic and/or -intrinsic function. Analysis of the intestinal permeability showed no significant difference between the increase in the DSS-induced clearance of the TRITC-dextran in the colon of Axin1$^{\Delta IEC}$ and WT mice, suggesting no specific alteration in the epithelial barrier integrity between the KO and WT mice upon the DSS challenge. This is in agreement with data showing that the systemic response to bacterial antigens can occur independently of epithelial barrier disruption.[42] These results favor an epithelium-intrinsic mechanism by which Axin1 promotes a proinflammatory response in the colon. From the RNA-seq/in silico analyses of both the tumors (Figure 10*A*, and Tables 1 and 2 in Figure 10) and the DSS-treated colon (Figure 11*C*, and Tables 3 and 4 in Figure 11), we can speculate that Axin1 participates in the transduction pathways that allow, under the sensing of microbial stimuli, the synthesis of immunoregulatory signals in the intestinal epithelial cells. In agreement with this hypothesis, a role for epithelial Axin1 in host–pathogen interactions has been described. *Salmonella typhimurium* decreases Axin1 protein expression in intestinal epithelial cell lines at the post-transcriptional level, whereas its overexpression inhibits *Salmonella* invasion bacterial infections in vitro.[43]

The RNA-seq data identified IFNγ/Stat1 and TNFα as the inflammatory pathways targeted by epithelial Axin1. This is consistent with the phenotype of mice with a genetic or a pharmacologic inhibition of *Stat1* that showed a decrease in the Th1 response and a reduction in chemically induced colitis.[44,45] Strikingly, the specific deletion of *Stat1* in intestinal epithelial cells phenocopied Axin1$^{\Delta IEC}$ mice and showed a tumor-suppressor function of Stat1 in CRC. Stat1$^{\Delta IEC}$ mice were more resistant to DSS-induced colitis and showed an increased tumor load upon the AOM/DSS protocol.[46] The mechanism by which epithelial Axin1 is able to activate the inflammatory pathways IFNγ/Stat1 and TNFα is largely unknown at present. Axin1 is a scaffolding protein for which many interactors have been described (https://www.ncbi.nlm.nih.gov/gene/8312) and has not yet been connected to any inflammatory pathway. Among the already identified interactors, Card9 and Traf2 have been implicated in intestinal inflammatory responses and cancer,[47,48] and may represent candidates meriting investigation.

Interestingly, the immune landscape has prognostic value[49]; notably, the features of the tumor microenvironment such as a lack of T-cell infiltration, and low levels of Th1 cell activity resulting in low levels of immune cytotoxicity, are predictive of adverse outcomes in patients with CRC; conversely, the presence of cytotoxic immune infiltration has been identified as a favorable prognostic marker.[27,50] RNA-seq and flow cytometry analyses of tumors from *Axin1*-deficient mice predicted a tumor microenvironment with low levels of IFNγ/Th1 cell activity. We therefore investigated whether the *Axin1*-dependent gene signature that we identified was of prognostic value in human CRC. In our 2239-sample series, the *Axin1* signature-based classification was found to be an independent prognostic feature: patients from the Axin1-proficient-like group had a longer DFS than those from the Axin1-deficient-like group. The difference in 5-year DFS was small (5%) between the 2 groups, but was significant in multivariate analysis. These Axin1-proficient-like patients also had molecular traits suggestive of a significantly stronger Th1/IFNγ/cytotoxic antitumor response that would make them more likely to respond to immunotherapy than Axin1-deficient-like patients and opens up possibilities for treatment. First, patients with the Axin1-proficient-like signature were enriched for CMS1 class, which is associated with a microsatellite instability -high status and predicted to respond best to immunotherapy, and thus might be expected to benefit from immune checkpoint blockade. Second, the use of tankyrase inhibitors could be optimized; these drugs stabilize Axin proteins[5] and have emerged as promising treatments for CRC,[6] although their clinical use is limited by their toxicity. The combined use of an immunotherapy approach together

Figure 9. (***See previous page***). ***Axin1* deficiency attenuates DSS-induced colitis.** (*A*) Body weight changes after treatment with 3% DSS or regular water (control) in WT (Axin1$^{fl/fl}$) and KO (Axin1$^{\Delta IEC}$) mice. WT ($n = 9$ for water, $n = 15$ for DSS) and KO ($n = 10$ for water, $n = 15$ for DSS) mice. (*B*) H&E staining of representative sections of colon after DSS treatment for WT and KO mice on days 7 and 13. Colon lengths after treatment with DSS or regular water of WT ($n = 9$) and KO ($n = 7$) mice. (*C*) H&E-stained images and histologic scores for colon sections after DSS treatment for WT and KO mice on days 7 and day 13. Histologic scores for colitis obtained for the WT and KO groups after treatment with DSS. *Scale bar*: 1 mm (*D*) Intestinal permeability assessed by fluorescein isothiocyanate (FITC)-dextran assay on day 5 of DSS administration (N = 5 per group). (*E*) Relative messenger RNA (mRNA) levels for *Axin1*, *Il6*, *Il1*β, *Tnf*α, *Ccl2*, and *Cxcl10* assessed by qRT-PCR analysis of the colon of DSS-treated mice killed on day 7 (WT, $n = 5$; KO, $n = 9$) or day 13 (WT, $n = 6$; KO, $n = 6$), and of mice given regular water (WT, $n = 9$; KO, $n = 10$). Significant differences as follows: *$P < .05$, **$P < .01$, ***$P < .001$, and ****$P < .0001$.

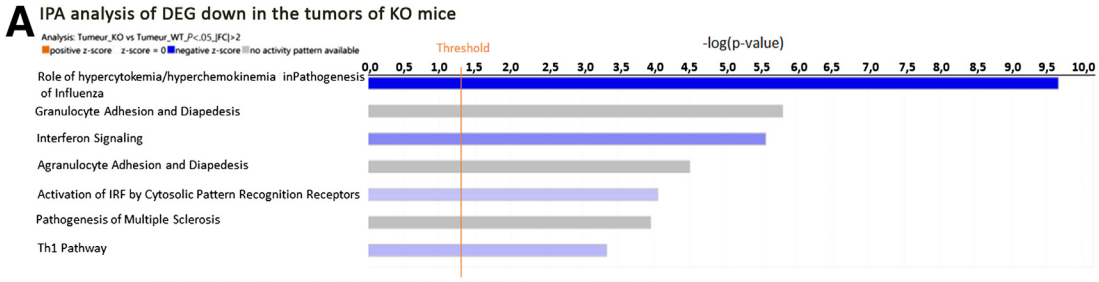

Table 2: ClueGo analysis of DEG down in the tumors of KO mice

ID	Term	Group *P*Value Corrected with Bonferroni step down
WP:1253	Type II interferon signaling (IFNG)	3,73E-07
KEGG:04620	Toll-like receptor signaling pathway	3,52E-07
KEGG:04621	NOD-like receptor signaling pathway	3,52E-07
KEGG:04657	IL-17 signaling pathway	3,73E-07
KEGG:04668	TNF signaling pathway	3,73E-07

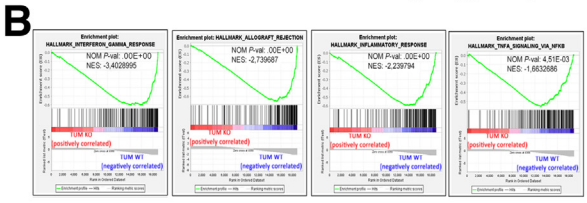

Table 3 : Upstream regulators identified by IPA

Upstream Regulator	Predicted Activation State	Activation z-score	*P*-value of overlap
STAT1	Inhibited	-6,568	7,41E-46
IFNAR1	Inhibited	-4,491	2,41E-39
IRF7	Inhibited	-6	2,81E-37
IRF3	Inhibited	-6,138	5,72E-37
IFNB1	Inhibited	-5,576	2,36E-35
IFNG	Inhibited	-7,41	9,89E-31
SOCS1	Activated	5,28	3,48E-29
Interferon alpha	Inhibited	-6,013	2,46E-26
IFN Beta	Inhibited	-4,016	1,42E-25
STAT3		0,356	2,45E-23

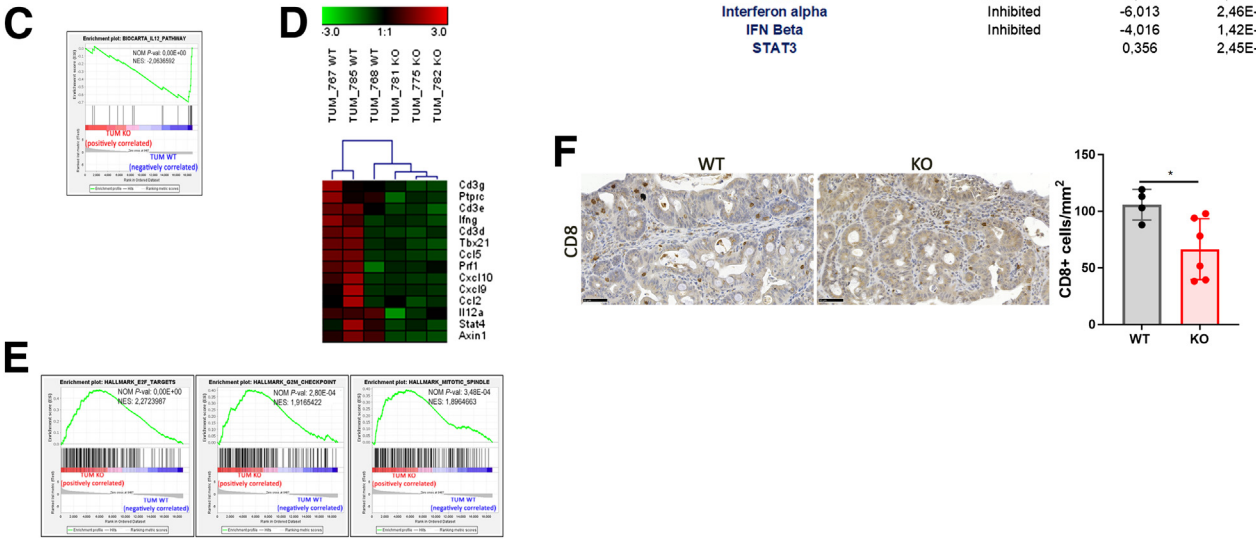

Figure 10. Functional gene expression profiling of AOM/DSS-induced colon tumors in Axin1$^{\Delta IEC}$ mice and controls. AOM/DSS-induced colon tumors from WT and KO mice were subjected to RNA-seq ($n = 3$ mice per group). (*A*) IPA analysis of DEGs down-regulated in the tumors of KO mice relative to the tumors of WT mice. The graph illustrates the most enriched pathways displaying down-regulation in the tumors of KO mice. Significance is expressed as the –log10 of *P* values. (*B*) GSEA results, by the Molecular Signatures Database (MSigDB) Hallmark gene set, showing negative enrichment in inflammatory and immune pathways in the tumors of KO mice. (*C*) GSEA, by the MSigDB Biocarta gene set, showing negative enrichment for the IL12 pathway in the tumors of KO mice. (*D*) Heatmap showing down-regulation of the IFNγ/Th1 immune response in the tumors of KO mice. (*E*) GSEA showing positive enrichment in cell-cycle pathways in the tumors from KO mice. (*F*) CD8 infiltration in tumors. Representative CD8$^+$ immunostainings of WT and KO colon tumors. *Scale bar*: 50 μm. Quantification of the CD8$^+$ T cells per mm^2 tumor tissue in WT and KO mice (N = 3 per group). Significant differences as follows: *$P < .05$. IRF, Interferon Regulator Factor; KEGG, Kyoto Encyclopedia of Genes and Genomes; NES, normalized enrichment score; NOD, nucleotide-binding oligomerization domain; NOM, nominal; TUM, Tumor; WP, Wikipathway.

with tankyrase inhibitors might be expected to lower the effective concentration range for the use of these inhibitors, at least in the group of patients bearing the Axin1-proficient-like signature.

In conclusion, our study showed a new mechanism by which Axin1 has tumor-suppressive function in CRC, which might open new therapeutic perspectives in colorectal cancer.

Materials and Methods

Ethical Compliance Statement

All animal procedures were performed according to French legal regulations (*Ministère de la Recherche, de l'Enseignement Supérieur et de l'Innovation*), with the approval of the Ethics Committee of Paris Descartes University (Project autorisation pour projets utilisant

animaux à des fins scientifiques [APAFIS] 8722 and 8612).

The human in silico study is based on public data from published studies in which the informed patients' consent to participate and the ethics and institutional review board already were obtained by authors. The study was approved by our Institutional Review Board from Institut Paoli-Calmettes (Marseille, France; Comité d'Orientation Stratégique).

Mice

Mice with an inducible specific deletion of *Axin1* in intestinal epithelial cells ($Axin1^{\Delta IEC}$) were obtained by crossing $Axin1^{fl/fl}$ mice[9] with Villin Cre-ERT2 mice expressing an inducible Cre-recombinase under the control of the villin promoter.[51] *Axin2*-null mice[16] were obtained from Anne-Amandine Chassot (Nice, France). For all experiments, approximately equal numbers of male and female mice were analyzed.

Mice were housed in colony cages in specific pathogen-free conditions, under a 12-hour light/dark cycle, in a controlled-temperature environment (21°C). They were fed ad libitum with a standard laboratory chow diet (65% carbohydrate, 11% lipids, and 24% proteins; SAFE 03, FRANCE).

Unless otherwise specified, we injected 4 doses of tamoxifen, 1 per day for 4 days (1 mg/mouse of tamoxifen, T5648; Sigma-Aldrich) in corn oil IP into 8- to 12-week-old mice.

For the inactivation of *Axin1* in hepatocytes, Ad5-CMV-cre and Ad5-GFP (2×10^9 plaque forming unit in 150 mL) were injected into the retro-orbital vein of 8-week-old mice anesthetized by isoflurane inhalation as previously described.[19]

DSS-Induced Colitis and Histologic Score

This experiment was performed as previously described.[52] Six- to 8-week-old WT ($Axin1^{fl/fl}$) and KO ($Axin1^{\Delta IEC}$) mice received 3% DSS (weight/volume) in drinking water for 7 days and then were given regular drinking water until they were killed. Mice from each strain and gender were kept in separate cages. Mice were monitored daily for weight loss and clinical disease (soft feces).

A histologic score was obtained according to the criteria described by Erben et al[53] based on inflammation, hyperplasia, epithelial damage, and mucosal architecture.

Induction of Colorectal Carcinogenesis

Colorectal tumorigenesis was induced in mice with the AOM-plus-DSS model, as previously described.[22] Briefly, 6- to 8-week-old WT ($Axin1^{fl/fl}$) and KO ($Axin1^{\Delta IEC}$) mice received a single IP injection of AOM (10 mg/kg body weight; Sigma). Mice from different strains and sexes were kept in separate cages. Over the next few weeks, mice were exposed to 3 cycles of treatment with 2.5% DSS (weight/volume) in drinking water for 7 days, with a 14-day interval in which the mice received regular water between cycles, for recovery. Mice were killed on day 100 after AOM injection.

Immunoblot Analysis

Total protein extracts were obtained from 100 mg frozen mouse liver or from mouse primary hepatocytes homogenized in lysis buffer (50 mmol/L Tris-HCl, pH 7.5, 150 mmol/L NaCl, 5 mmol/L EDTA, 30 mmol/L $Na_4P_2O_7$, 50 mmol/L Sodium fluoride [NaF], 1% Triton X-100 [Sigma-Aldrich], 1 mmol/L dithiothreitol) protease inhibitor cocktail (32953; Pierce, Thermo Fisher Scientific) supplemented with phosphatase inhibitor cocktail (8867; Pierce, Thermo Fisher Scientific) in a bead mill, with the Tissue Lyser disruption system (Qiagen, Hilden, Germany). Proteins were resolved by sodium dodecyl sulfate–polyacrylamide gel electrophoresis. The resulting bands were transferred to nitrocellulose membranes, which were blocked by incubation with 5% bovine serum albumin or 5% milk. Blots were incubated overnight at 4°C with specific primary antibodies, washed, incubated with the corresponding horseradish-peroxidase–conjugated secondary antibodies (Cell Signaling), and developed by an enhanced chemiluminescence technique (Thermo Fisher Scientific). Primary antibodies were obtained from Cell Signaling Technologies (Axin1, ref: C76H11, 1:500) and Santa Cruz Biotechnology (glyceraldehyde-3-phosphate dehydrogenase [Gapdh], ref: sc-25778, 1:1000).

Histology and Immunohistochemistry

Immediately after death, the entire gastrointestinal tract of the mouse was removed, splayed open along its length, and rolled up from the proximal to the distal end to form a Swiss roll. Tissues were fixed by incubation in 4% paraformaldehyde overnight at 4°C and embedded in paraffin wax. Sections (3-μm thick) were cut and stained with H&E. Immunohistochemistry was performed as previously described.[54] We treated 5-μm sections with 3% hydrogen peroxide for 15 minutes at room temperature. Antigens then were retrieved by boiling for 15 minutes in citrate buffer (10 mmol/L, pH 6) or for 40 minutes in Tris-EDTA buffer (100 mmol/L Tris, 12.6 mmol/L, pH 9) in a microwave pressure cooker (EZ Retriever; Biogenex). The sections were incubated in blocking solution (2% goat serum, 1% bovine serum albumin diluted in Tris Buffer Saline Tween) for 20 minutes at room temperature. They then were incubated overnight at 4°C with the primary antibodies against the following proteins, diluted in blocking solution: cleaved caspase-3 (9661S, 1:200; Cell Signaling), Ki-67 (12202S, 1:1500; Cell Signaling), lysozyme (EC.3.2.1.17, 1:200; Dako), Olfm4 (CS 39141S, 1:400; Cell Signaling), p53 (NCL-p53-CM5p, 1:200; Leica), γH2AX (05-636, 1:300; Millipore), chromogranin B (HPA012602, 1:1000; Atlas Antibodies), villin (ab130751, 1:500; Abcam), glutamine synthetase (610518, 1:400; BD Biosciences), and CD8 (14-0808-80, 1:100; eBiosciences). Specific binding was detected with a biotinylated secondary antibody and ABC reagent (Vector) for immunohistochemistry, and the signal was revealed with 3,3′-diaminobenzidine tetra hydrochloride solution (Vector). Hematoxylin was used as a nuclear counterstain.

Apoptosis was assessed with a TUNEL assay kit, in accordance with the manufacturer's instructions (QIA33; Calbiochem). In the crypt, the 5–6 cells located above the +4 cells were considered transit-amplifying cells.

Quantification of the labeled positive cells was performed in almost 40 consecutive crypts in the small intestine and in 20 consecutive crypts in the colon. This provides an average of positive cells in the crypts per animal.

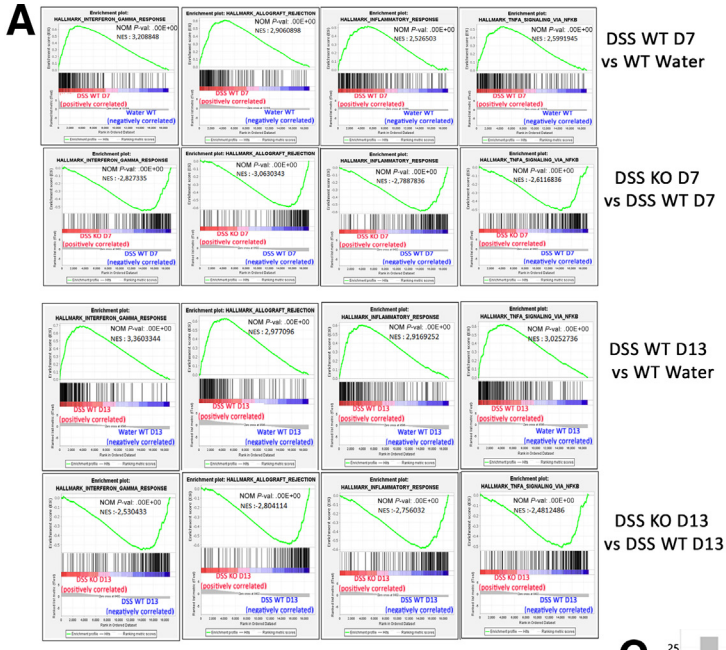

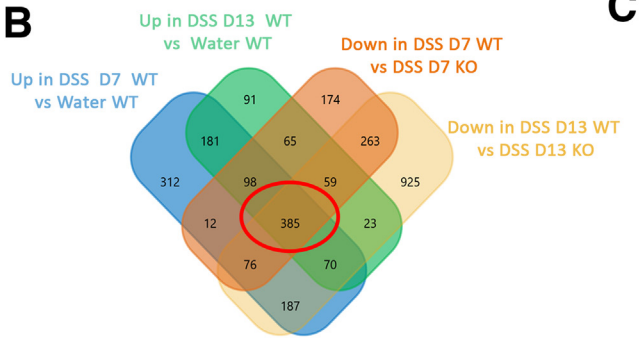

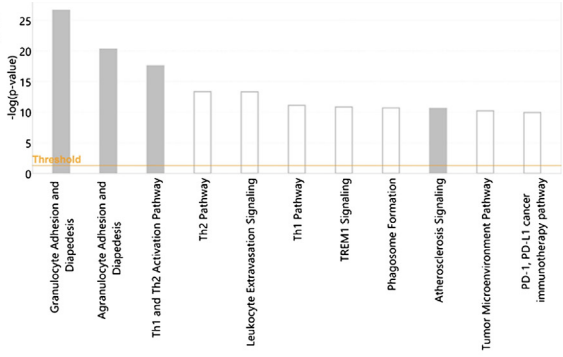

Table 4: CueGo analysis of the 385 genes

ID	Term	Group PValue Corrected with Bonferroni step down
R-MMU:1280218	Adaptive Immune System	2,29E-31
R-MMU:168249	Innate Immune System	2,29E-31
KEGG:04658	Th1 cell differentiation	1,32E-27
KEGG:04659	Th17 cell differentiation	1,32E-27

Table 5: Upstream regulators identified by IPA

Upstream Regulator	*P*-value of overlap
lipopolysaccharide	1,56E-93
IFNG	6,36E-79
STAT1	1,49E-43
STAT3	2,13E-42
NFkB (complex)	2,07E-37

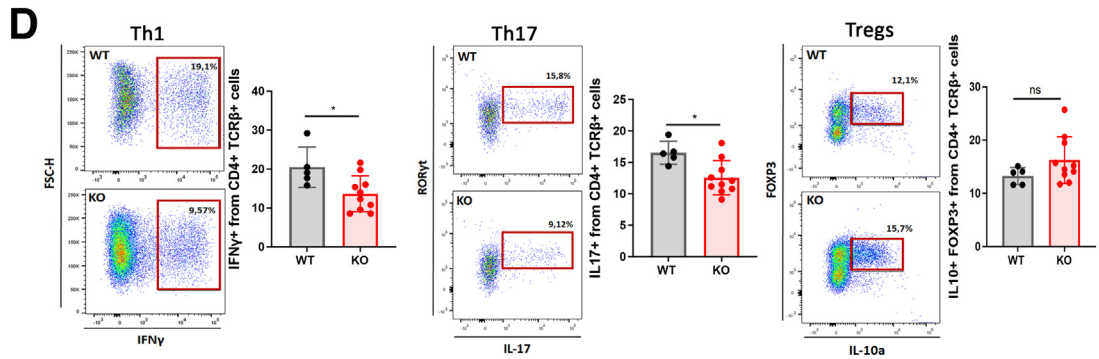

Table 1. Description of the 11 Human Colon Cancer Data Sets Included

Study	Data source	Technological platform	Probe sets/genes, n	Colon samples, n	Primary colon cancers, n
Jorissen et al, Clin Cancer Res 2009. PMID: 19996206	GEO database: GSE14333	Array U133 Plus 2.0; Affymetrix	54,000	251	251
Sheffer et al, Proc Natl Acad Sci U S A 2009. PMID: 19359472	GEO database: GSE41258	Array U133 A; Affymetrix	22,000	289	168
Staub et al, J Mol Med (Berl) 2009. PMID: 19399471	GEO database: GSE12945	Array U133 Plus 2.0; Affymetrix	54,000	29	29
Smith et al, Gastroenterology 2010. PMID: 19914252	GEO database: GSE17538	Array U133 Plus 2.0; Affymetrix	54,000	232	232
de Sousa et al, Cell Stem Cell 2011. PMID: 22056143	GEO database: GSE33113	Array U133 Plus 2.0; Affymetrix	54,000	90	90
Kenned et al, J Clin Oncol 2011. PMID: 22067406	Array-Express database: E-MTAB-863	Custom array: ADXCRCG2a520319; Affymetrix	62,000	215	215
Sveen et al, Genome Med 2011. PMID: 21619627	GEO database: GSE24551	Human Exon 1.0 ST array; Affymetrix	22,000	160	160
Laibe et al, OMICS 2012. PMID: 22917480	GEO database: GSE37892	Array U133 Plus 2.0; Affymetrix	54,000	130	130
Marisa et al, PLoS Med 2013. PMID: 23700391	GEO database: GSE39582	Array U133 Plus 2.0; Affymetrix	54,000	455	455
TCGA, COAD	TCGA portal: https://tcga-data.nci.nih.gov	RNA sequencing V2; Illumina	25,000	500	459
IPC	Ongoing submission to ArrayExpress	Array U133 Plus 2.0; Affymetrix	54,000	50	50
Total					2239

COAD, Colon adenocarcinoma; IPC, Institut Paoli-Calmettes; TCGA, The Cancer Genome Atlas.

Quantification was performed on 3 or 4 different mice in each group and statistics were performed on these combined averaged numbers.

Mouse livers were cut into 3-mm–thick sections and fixed by incubation in 4% paraformaldehyde for 12 hours. They then were embedded in paraffin. Immunohistochemistry was

Figure 11. (***See previous page***). **Functional gene expression profiling of the colon after acute DSS treatment in Axin1$^{\Delta IEC}$ mice and controls.** Colon tissues from WT and KO mice treated with DSS for 5 days and killed on day 7 (D7) or day 13 (D13), and colon tissue from WT untreated mice, were subjected to RNA-seq ($n = 3$ mice per group). (*A*) GSEA results, by Molecular Signatures Database Hallmark gene set, showing a positive enrichment in inflammatory and immune pathways in colonic tissues from WT mice treated with DSS on day 7 (D7) and D13 (D13) relative to untreated WT mice receiving water (*top*), and an inverse negative enrichment in these pathways in DSS-treated KO samples relative to DSS-treated WT samples (*bottom*). (*B*) Venn diagram showing the number of DEGs up-regulated in WT DSS-treated mice relative to untreated WT mice both on D7 and D13, together with the number of DEGs down-regulated in the KO DSS-treated mice relative to the WT DSS-treated mice both on D7 and D13. A total of 385 genes were identified as commonly up-regulated in WT DSS-treated mice relative to untreated WT and down-regulated in the KO DSS-treated mice relative to the WT DSS-treated mice. (*C*) IPA analysis of the 385 genes up-regulated in DSS-treated WT mice and down-regulated in DSS-treated KO mice. (*D*) fluorescence-activated cell sorting (FACS) analysis of of T-cell effector cell responses from colonic lamina propria of DSS-treated mice. T-cell populations in freshly isolated immune cells from the lamina propria of the colon of *Axin*-deficient (KO) mice and WT mice treated by DSS and killed on D13 were analyzed by FACS analyses. Representative flow cytometry plots of IFNγ^+ cells within CD4$^+$Tcrβ^+ (Th1) cells, of Rorγt$^+$Il17$^+$ T cells within CD4$^+$Tcrβ^+ cells (Th17) and of Foxp3$^+$Il10a$^+$ within CD4$^+$Tcrβ^+ cells (regulatory T cell [Treg]) cells from WT mice and KO mice are shown. Box plots quantifying the percentage of IFNγ^+ (Th1), Rorγt$^+$Il17$^+$ (Th17), and Foxp3$^+$Il10a$^+$ (Treg) cells within the CD4$^+$Tcrβ^+ cell population (means ± SEM; WT, n = 5; KO, n = 10). Significant differences as follows: $^*P < .05$. FOXP3, forkhead box P3; FSC-H, Forward side scatter-Height; IFNG, interferon gamma; KEGG, Kyoto Encyclopedia of Genes and Genomes; NES, normalized enrichment score; NOM, nominal; PD-1, programmed cell death 1; PD-L1, CD274 molecule; R-MMU, Reactome pathway; RORγt,RAR-related orphan receptor gamma t; TREM1, Triggering receptor expressed on myeloid cells 1.

Table 2. Clinical and Pathologic Characteristics of the Colon Cancer Samples for the Whole Series and According to Axin1-Proficient-Like Vs Axin1-Deficient-Like Status

Characterist	N	All	*Axin1* proficient-like	*Axin1* deficient-like	*P* value
Age, *y*					.606
≤50	228	228 (12%)	110 (12%)	118 (11%)	
>50	1702	1702 (88%)	786 (88%)	916 (89%)	
Sex					**2.71E-02**
Female	954	954 (47%)	469 (50%)	485 (45%)	
Male	1069	1069 (53%)	472 (50%)	597 (55%)	
Site					**3.21E-09**
Distal	840	840 (50%)	328 (42%)	512 (56%)	
Proximal	854	854 (50%)	457 (58%)	397 (44%)	
Stage[a]					**1.17E-04**
1	167	167 (10%)	80 (10%)	87 (10%)	
2	667	667 (41%)	342 (45%)	325 (38%)	
3	548	548 (34%)	264 (34%)	284 (33%)	
4	237	237 (15%)	81 (11%)	156 (18%)	
MMR status					**1.43E-05**
dMMR	128	128 (19%)	79 (26%)	49 (13%)	
pMMR	563	563 (81%)	226 (74%)	337 (87%)	
CMS subtype					**1.67E-47**
CMS1	389	389 (20%)	295 (30%)	94 (9%)	
CMS2	640	640 (32%)	187 (19%)	453 (46%)	
CMS3	343	343 (17%)	170 (17%)	173 (17%)	
CMS4	604	604 (31%)	332 (34%)	272 (27%)	
DFS event, N (%)	1843	594 (32)	256 (29)	338 (36)	**1.41E-03**
5-year DFS	1843	66% [63–68]	68% [65–72]	63% [60–67]	**1.69E-02**

NOTE: bold text specifies significant value of each analyzed parameter.
dMMR, deficient mismatch repair.
[a]Pathologic stage (based on patholofgc stage Tumor, pathologic stage Mode, and Metastasis).

performed as previously described.[19] An antibody against glutamine synthetase was used (610518, 1:400; BD Biosciences).

Intestinal Permeability

Four hours (average time of intestinal transit in mice) before killing, overnight fasted mice were orally gavaged with a solution of TRITC dextran 4 kilodaltons at 50 mg/mL in phosphate-buffered saline (PBS) (TdB Labs, Sweden). Blood then was collected at the tail tip. Plasma was analyzed for the TRITC dextran 4 kilodalton concentration using an automatic fluorescence microplate reader at 544-nm excitation and 580-nm emission wavelengths to determine the intestinal epithelium permeability. TRITC concentrations were determined using standard curves prepared by diluting various amounts of TRITC-dextran in PBS.

RNA Extraction and Quantitative Real-Time PCR Analysis

Total RNA was extracted from mouse tissues with TRIzol Reagent (Life Technologies) in accordance with the manufacturer's protocol. Reverse-transcription was performed with 1 μg total RNA and the Transcriptor First-Strand Complementary DNA Synthesis Kit (Roche Diagnostics), with random hexamer primers. Quantitative PCR was performed with the Light Cycler 480 Sybr Green I Master kit (Roche) and specific primers (Eurogentec) on a Light Cycler 480 thermocycler (Roche). RNA levels were calculated by the $2^{(-\text{Delta Ct})}$ method, with 18S as the internal control, relative to RNA levels in control ($Axin1^{fl/fl}$) mice.

RNA-Seq Analysis

RNA extracted from colon tissue (distal colon) was treated with DNAse1 according to the manufacturer's protocol (RNA Clean and Concentrator-5, R1013; Zymo Research). Three different mice per genotype were used for RNA-seq analysis. Library preparation and sequencing were performed at the GenomIC' sequencing facility using 3 RNA samples per genotype (https://www.institutcochin.fr/core_facilities/genomesequencing-studies). The libraries were prepared following the TruSeq Stranded messenger RNA protocol from Illumina, starting from 800 ng high-quality total RNA (RNA Integrity Number, >8). Paired-end (2 × 75 bp) sequencing was performed on an Illumina Nextseq 500 platform, 20–40 millions paired end reads were used for the analysis. After sequencing, a primary analysis was performed with AOZAN software (ENS, Paris) for demultiplexing and quality control analysis on the raw data (based on FastQC modules, version 0.11.5).

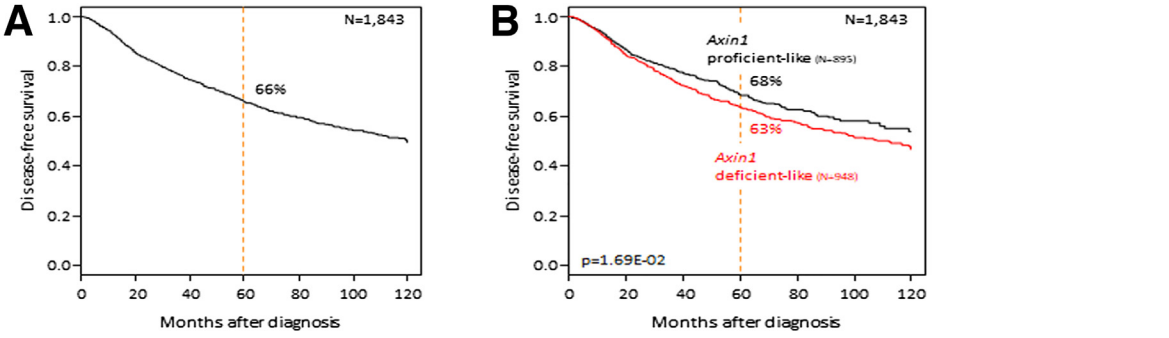
A
N=1,843
66%
Disease-free survival
Months after diagnosis
B
N=1,843
Axin1
proficient-like (N=895)
68%
63%
Axin1
deficient-like (N=948)
p=1.69E-02
Disease-free survival
Months after diagnosis

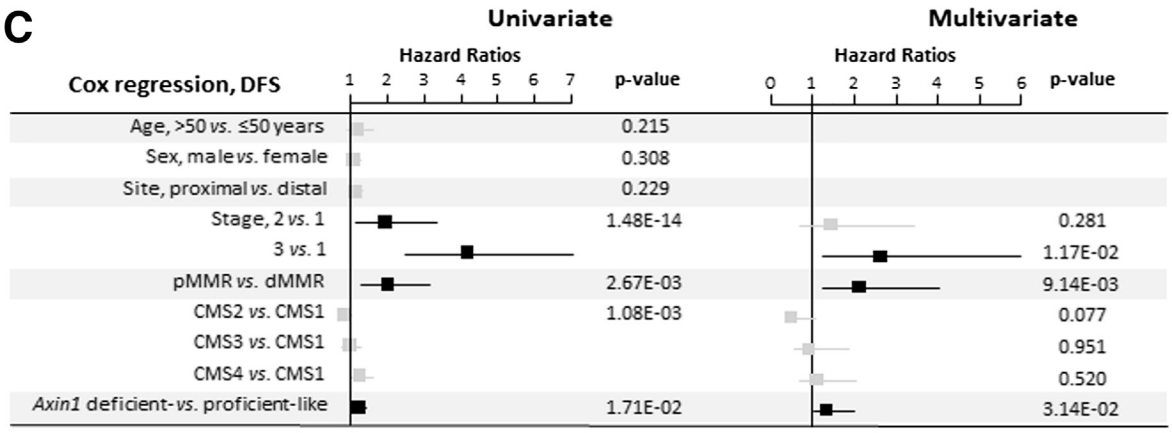
C
Univariate
Multivariate
Cox regression, DFS
Hazard Ratios
p-value
Age, >50 vs. ≤50 years 0.215
Sex, male vs. female 0.308
Site, proximal vs. distal 0.229
Stage, 2 vs. 1 1.48E-14 0.281
3 vs. 1 1.17E-02
pMMR vs. dMMR 2.67E-03 9.14E-03
CMS2 vs. CMS1 1.08E-03 0.077
CMS3 vs. CMS1 0.951
CMS4 vs. CMS1 0.520
Axin1 deficient- vs. proficient-like 1.71E-02 3.14E-02

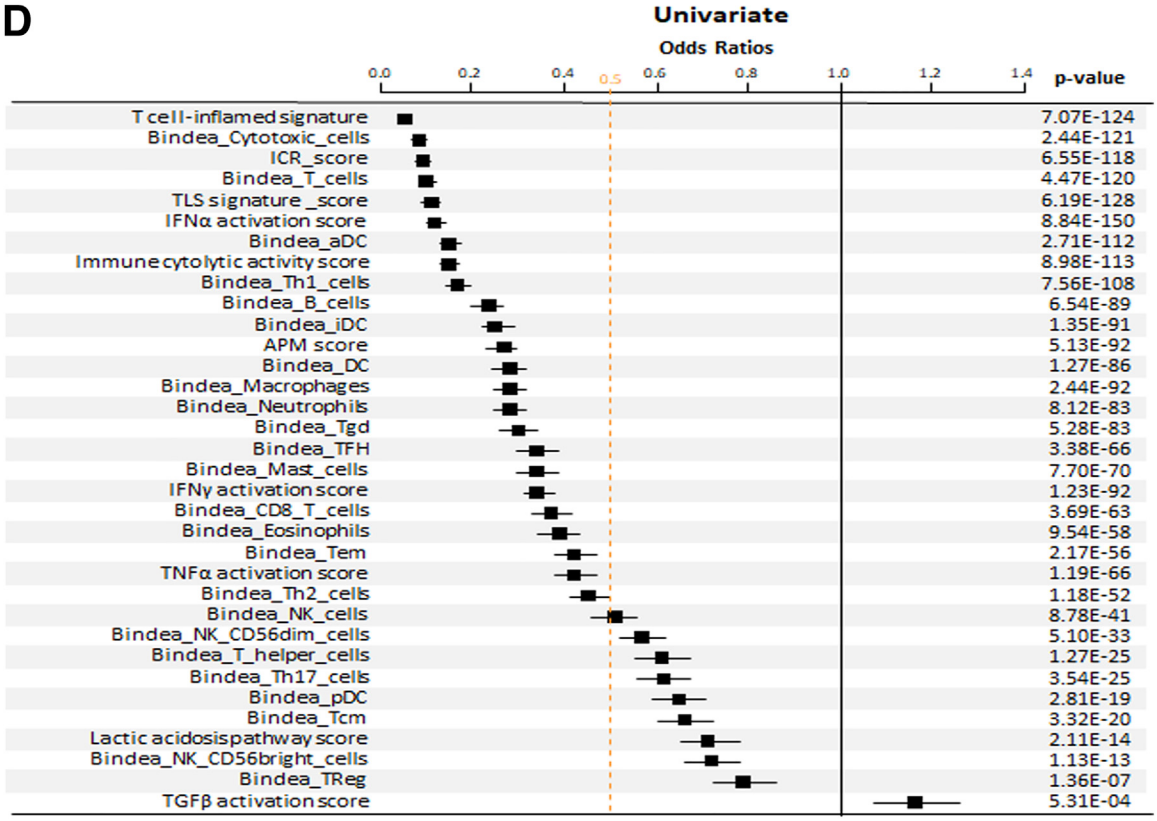
D
Univariate
Odds Ratios
p-value
T cell-inflamed signature 7.07E-124
Bindea_Cytotoxic_cells 2.44E-121
ICR_score 6.55E-118
Bindea_T_cells 4.47E-120
TLS signature _score 6.19E-128
IFNα activation score 8.84E-150
Bindea_aDC 2.71E-112
Immune cytolytic activity score 8.98E-113
Bindea_Th1_cells 7.56E-108
Bindea_B_cells 6.54E-89
Bindea_iDC 1.35E-91
APM score 5.13E-92
Bindea_DC 1.27E-86
Bindea_Macrophages 2.44E-92
Bindea_Neutrophils 8.12E-83
Bindea_Tgd 5.28E-83
Bindea_TFH 3.38E-66
Bindea_Mast_cells 7.70E-70
IFNγ activation score 1.23E-92
Bindea_CD8_T_cells 3.69E-63
Bindea_Eosinophils 9.54E-58
Bindea_Tem 2.17E-56
TNFα activation score 1.19E-66
Bindea_Th2_cells 1.18E-52
Bindea_NK_cells 8.78E-41
Bindea_NK_CD56dim_cells 5.10E-33
Bindea_T_helper_cells 1.27E-25
Bindea_Th17_cells 3.54E-25
Bindea_pDC 2.81E-19
Bindea_Tcm 3.32E-20
Lactic acidosis pathway score 2.11E-14
Bindea_NK_CD56bright_cells 1.13E-13
Bindea_TReg 1.36E-07
TGFβ activation score 5.31E-04

The STAR algorithm (version 2.7.6a; Genomic'IC) then was used to align the Fastq files with the Ensembl Mus musculus GRCm38 reference, release 101 (Genomic'IC). Reads then were counted with RSEM (v1.3.1; Genomic'IC) and statistical analyses were performed on the read counts with R (version 3.6.3; Genomic'IC) and the DESeq2 package (DESeq2_1.26.0; Genomic'IC) to determine the proportion of genes differentially expressed between 2 conditions.

We used the standard DESeq2 normalization method (DESeq2 median of ratios with the DESeq function), with a prefilter of reads and genes (reads uniquely mapped on the genome, or up to 10 different loci with a count adjustment, and genes with at least 10 reads in at least 3 different samples).

In accordance with the recommendations for this package, we used the Wald test with the contrast function and the Benjamini–Hochberg false discovery rates control procedure to identify DEGs.

R scripts and parameters are available from GitHub (https://github.com/BSGenomique/genomic-Rnaseq-pipeline/releases/tag/v1.0420).

Ontology Analyses

The list of genes showing significant differential expression was explored by both over-representation and GSEAs.

Over-representation analysis was performed by Ingenuity Pathway Analysis (Qiagen, Inc, https://www.qiagenbioinformatics.com/products/ingenuitypathway-analysis) version 60467501 for canonical pathways and upstream regulators, and ClueGO v2.5.8 (http://www.ici.upmc.fr/cluego) for WikiPathways, Kyoto Encyclopedia of Genes and Genomes (KEGG), and Reactome pathways.

Significantly over-represented terms were identified with a right-tailed Fisher exact test, which calculated an overlap *P* value determining the probability of each term being associated with our lists of differential transcripts by chance alone.

The IPA z-score is a statistical measurement of correlation between the direction of the relationship and experimental levels of protein. It was calculated to assess the activation (positive z-score) or repression (negative score) of each term. The z-score was considered significant if its absolute value was greater than 2. GSEA was performed with Broad Institute GSEA software v4.1.0 (http://software.broadinstitute.org/gesa/index.jsp).[55] GSEA determined whether gene sets from the Molecular Signatures Database Hallmark collection (v7.4) were distributed randomly throughout our ranked transcript lists or whether they were located toward the top or bottom of these lists.

Heatmaps were generated with Genesis software (https://genome.tugraz.at).[56] Venn diagrams were produced with the FunRich functional enrichment analysis tool v3.1.3 (http://funrich.org).[57]

Flow Cytometric Analyses

Lymphocytes were extracted from lamina propria as previously described.[58] Briefly, small intestines were rinsed in cold PBS, minced into small pieces, incubated with EDTA (2 mmol/L), and digested with collagenase (1.5 mg/mL) for 30 minutes at 37°C. A discontinuous Percoll separation method (40% and 80%) was used to purify immune cells. Cell suspensions were centrifuged and the pellet was resuspended in 40% Percoll layered by 80% Percoll. The cells concentrated at the interface were collected and washed in cold PBS. Cells were suspended in RPMI1640 containing 5% fetal bovine serum, counted, incubated with human FcgammaR-binding inhibitor Receptor Binding Inhibitor Polyclonal Antibody (14-9161-73; eBioscience) and stained with specific antibodies.

Cells were subjected to fluorescence-activated cell sorting (FACS) analysis with the following antibodies: anti-CD4 (RM4-5 clone, 558107; BD Biosciences), anti-CD19 (1D3 clone, 550992; BD Biosciences) anti-IFNγ (XMG1.2 clone, 554412; BD Biosciences), or anti-transcription factor forkhead box P3 (FOXP3) (FJK-16s clone, 12-5773; eBioscience), anti-IL10 (JES5-16E3 clone, 554467; BD Biosciences), anti-IL17A (TC11-18H10 clone, 560220; BD Biosciences), and anti-RAR-related orphan receptor gamma (RORγ) (t) (REA278 clone, 130-123-248; Miltenyi Biotec). Dead cells were removed using the LIVE/DEAD Fixable Aqua Dead Cell Stain Kit (L34957; Invitrogen).

For intracellular staining, cells were pretreated with phorbol myristate acetate/ionomycin for 4 hours at 37°C 5% CO_2 and brefeldin A was added for the last 3 hours. Cells then were stained with specific extracellular antibodies, permeabilized with BD cytoFix/cytoPerm solution (555028; BD Biosciences) or with transcription factor staining buffer set (00-5523-00; eBiosicence), and, finally, stained intracellularly for IFNγ, IL10, RORγ(t), IL17, or Foxp3. FACS analysis was performed with the BD LSR Fortessa flow cytometer (BD Biosciences) with FlowJo software (BD Bioscience).

Gene Expression Analysis on Colon Cancer Clinical Samples

We assessed the biological and clinical relevance of our 327-gene signature (*Axin1*-deficient mice vs *Axin1*-proficient mice) in human CRC samples by analyzing our database

Figure 12. (***See previous page***). **Correlations of *Axin1*-proficient-like and *Axin1*-deficient-like colon cancers with DFS and molecular variables.** (*A*) Kaplan–Meier DFS curves for patients with surgically treated colon cancers. (*B*) As in panel *A*, but according to the *Axin1*-proficient-like and *Axin1*-deficient-like groups. The *P* value for the log-rank test is shown. (*C*) Forest plots of hazards ratios between the *Axin1*-proficient-like and *Axin1*-deficient-like groups in univariate and multivariate Cox analyses for DFS. The *P* values shown were obtained by the Wald test. (*D*) Forest plots of odds ratios between the *Axin1*-proficient-like and *Axin1*-deficient-like groups in univariate logistic regression analysis for molecular variables. The *P* values shown were obtained in logit link tests and the variables are ranked with *P* values increasing from top to bottom. aDC, activated DC; APM, Antigen presenting Machinery; DC, Dendritic cell; dMMR, deficient mismatch repair; ICR, Immunologic Constant of Rejection; iDC, immature DC; NK, Natural Killer; pDC, Plasmacytoid dendritic cell; Tem, T effector memory; TFH, T follicular helper; Tgd, _T gamma delta; TGF, transforming growth factor; TLS, _tertiary lymphoid structures; TReg, regulatory T cell.

including clinical, pathologic, and gene expression data for primary CRC samples from 10 publicly available data sets and our own data set generated at the Institut Paoli-Calmettes (Marseille, France). Data were collected from the National Center for Biotechnology Information/GenBank Gene Expression Ommnibus, ArrayExpress, and The Cancer Genome Atlas (TCGA) databases (Table 1). Samples were profiled with DNA microarrays (Affymetrix) or by RNA sequencing (Illumina). The data set analyzed contained data for 2239 primary CRC samples. The characteristics of these samples are summarized in Table 2. Briefly, 88% of patients were older than age 50 years, and 53% were male. The proximal colon was the site of the CRC in 51% of cases. There were more stage 2 cancers (41%) than stage 3 cancers (34%). MMR status was classified as pMMR in 81% of cases. CMS determination identified 20% of samples as CMS1 (microsatellite instability immune), 32% as CMS2 (canonical), 17% as CMS3 (metabolic), and 31% as CMS4 (mesenchymal). DFS data were available for 1843 non-metastatic patients with CMS subtyping data who had undergone surgery.

Data analysis required a preanalytical processing step, as previously described.[59] We then applied several multigene molecular signatures separately to each tumor in each data set. We first used the 327 DEGs between the tumors of *Axin1*-deficient mice and tumors from WT mice to define an *Axin1*-deficient vs *Axin1*-proficient expression profile. We then calculated the Pearson correlation distance between each sample and this profile: the samples with negative correlations were classified as *Axin1*-proficient-like ($N = 1053$) and those with positive correlations were classified as *Axin1*-deficient-like ($N = 1186$). The other gene expression signatures applied included the CMS classification,[60] the signatures of 24 different innate and adaptive immune cell subpopulations from Bindea et al,[28] the immune constant of rejection classifier,[30] metagenes associated with the T-cell–inflamed signature,[29] the tertiary lymphoid structures signature,[34] the cytolytic activity score,[31] the antigen processing/presentation machinery score,[33] and the pathway activation scores from Gatza et al.[32]

In statistical analysis, the correlations between the *Axin1*-proficient-like and *Axin1*-deficient-like groups and the clinical and pathologic variables were calculated with the Fisher exact test. The DFS was calculated from the date of diagnosis until the date of metastatic relapse or death from CRC. Follow-up evaluation was measured from the date of diagnosis to the date of last contact for event-free patients. Survival was calculated by the Kaplan–Meier method, and curves were compared in log-rank tests. Univariate and multivariate prognostic analyses for DFS were performed by Cox regression analysis (Wald test). The variables tested in univariate analysis included *Axin1*-proficient-like vs *Axin1*-deficient-like status, patient age (>50 y vs ≤50 y), sex (male vs female), tumor site (proximal vs distal), pathologic stage (2 vs 1, 3 vs 1), MMR status (pMMR vs deficient MMR), and CMS classification (CMS2 vs CMS1, CMS3 vs CMS1, and CMS4 vs CMS1). Multivariate analysis incorporated all variables with a P value less than 5% in univariate analysis. The correlations of molecular variables with *Axin1*-proficient-like and *Axin1*-deficient-like status were assessed by logistic regression analysis with the lm function (R statistical package; significance estimated by specifying a binomial family for models with a logit link). All statistical tests were 2-tailed and were performed with an α risk of 5%. Statistical analysis was performed with the survival package (version 2.43) in R software (version 3.5.2)

Statistical Analysis

Statistical analyses were performed with GraphPad Prism (9.04). Graphic data are represented as means ± SD unless specified. Data were checked for normality and unpaired 2-tailed Student t tests were used to assess differences between groups. P values less than .05 were considered significant.

References

1. Sung H, Ferlay J, Siegel RL, et al. Global cancer statistics 2020: GLOBOCAN estimates of incidence and mortality worldwide for 36 cancers in 185 countries. CA Cancer J Clin 2021;71:209–249.
2. Cancer Genome Atlas Network. Comprehensive molecular characterization of human colon and rectal cancer. Nature 2012;487:330–337.
3. de Sousa EMF, Vermeulen L. Wnt signaling in cancer stem cell biology. Cancers (Basel) 2016;8:60.
4. Mazzoni SM, Fearon ER. AXIN1 and AXIN2 variants in gastrointestinal cancers. Cancer Lett 2014;355:1–8.
5. Huang SM, Mishina YM, Liu S, et al. Tankyrase inhibition stabilizes axin and antagonizes Wnt signalling. Nature 2009;461:614–620.
6. Lau T, Chan E, Callow M, et al. A novel tankyrase small-molecule inhibitor suppresses APC mutation-driven colorectal tumor growth. Cancer Res 2013;73:3132–3144.
7. Zucman-Rossi J, Villanueva A, et al. Genetic landscape and biomarkers of hepatocellular carcinoma. Gastroenterology 2015;149:1226–1239 e4.
8. Satoh S, Daigo Y, Furukawa Y, et al. AXIN1 mutations in hepatocellular carcinomas, and growth suppression in cancer cells by virus-mediated transfer of AXIN1. Nat Genet 2000;24:245–250.
9. Abitbol S, Dahmani R, Coulouarn C, et al. AXIN deficiency in human and mouse hepatocytes induces hepatocellular carcinoma in the absence of beta-catenin activation. J Hepatol 2018;68:1203–1213.
10. Zeng L, Fagotto F, Zhang T, et al. The mouse fused locus encodes Axin, an inhibitor of the Wnt signaling pathway that regulates embryonic axis formation. Cell 1997;90:181–192.
11. Kishida S, Yamamoto H, Ikeda S, et al. Axin, a negative regulator of the Wnt signaling pathway, directly interacts with adenomatous polyposis coli and regulates the stabilization of beta-catenin. J Biol Chem 1998;273:10823–10826.
12. Clevers H, Nusse R. Wnt/beta-catenin signaling and disease. Cell 2012;149:1192–1205.
13. Salahshor S, Woodgett JR. The links between axin and carcinogenesis. J Clin Pathol 2005;58:225–236.

14. Lin SC, Hardie DG. AMPK: sensing glucose as well as cellular energy status. Cell Metab 2018; 27:299–313.
15. Bohin N, Carlson EA, Samuelson LC. Genome toxicity and impaired stem cell function after conditional activation of CreER(T2) in the intestine. Stem Cell Rep 2018; 11:1337–1346.
16. Yu HM, Jerchow B, Sheu TJ, et al. The role of Axin2 in calvarial morphogenesis and craniosynostosis. Development 2005;132:1995–2005.
17. Andreu P, Colnot S, Godard C, et al. Crypt-restricted proliferation and commitment to the Paneth cell lineage following Apc loss in the mouse intestine. Development 2005;132:1443–1451.
18. Adam RS, van Neerven SM, Pleguezuelos-Manzano C, et al. Intestinal region-specific Wnt signalling profiles reveal interrelation between cell identity and oncogenic pathway activity in cancer development. Cancer Cell Int 2020;20:578.
19. Benhamouche S, Decaens T, Godard C, et al. Apc tumor suppressor gene is the "zonation-keeper" of mouse liver. Dev Cell 2006;10:759–770.
20. Cadoret A, Ovejero C, Terris B, et al. New targets of beta-catenin signaling in the liver are involved in the glutamine metabolism. Oncogene 2002;21:8293–8301.
21. Colnot S, Decaens T, Niwa-Kawakita M, et al. Liver-targeted disruption of Apc in mice activates beta-catenin signaling and leads to hepatocellular carcinomas. Proc Natl Acad Sci U S A 2004;101:17216–17221.
22. Neufert C, Becker C, Neurath MF. An inducible mouse model of colon carcinogenesis for the analysis of sporadic and inflammation-driven tumor progression. Nat Protoc 2007;2:1998–2004.
23. Takahashi M, Nakatsugi S, Sugimura T, Wakabayashi K. Frequent mutations of the beta-catenin gene in mouse colon tumors induced by azoxymethane. Carcinogenesis 2000;21:1117–1120.
24. Neurath MF. Cytokines in inflammatory bowel disease. Nat Rev Immunol 2014;14:329–342.
25. Dunn GP, Koebel CM, Schreiber RD. Interferons, immunity and cancer immunoediting. Nat Rev Immunol 2006;6:836–848.
26. Kim R, Emi M, Tanabe K. Cancer immunoediting from immune surveillance to immune escape. Immunology 2007;121:1–14.
27. Galon J, Costes A, Sanchez-Cabo F, et al. Type, density, and location of immune cells within human colorectal tumors predict clinical outcome. Science 2006; 313:1960–1964.
28. Bindea G, Mlecnik B, Tosolini M, et al. Spatiotemporal dynamics of intratumoral immune cells reveal the immune landscape in human cancer. Immunity 2013; 39:782–795.
29. Ayers M, Lunceford J, Nebozhyn M, et al. IFN-gamma-related mRNA profile predicts clinical response to PD-1 blockade. J Clin Invest 2017;127:2930–2940.
30. Bertucci F, Finetti P, Simeone I, et al. The immunologic constant of rejection classification refines the prognostic value of conventional prognostic signatures in breast cancer. Br J Cancer 2018;119:1383–1391.
31. Rooney MS, Shukla SA, Wu CJ, et al. Molecular and genetic properties of tumors associated with local immune cytolytic activity. Cell 2015;160:48–61.
32. Gatza ML, Lucas JE, Barry WT, et al. A pathway-based classification of human breast cancer. Proc Natl Acad Sci U S A 2010;107:6994–6999.
33. Thompson JC, Davis C, Deshpande C, et al. Gene signature of antigen processing and presentation machinery predicts response to checkpoint blockade in non-small cell lung cancer (NSCLC) and melanoma. J Immunother Cancer 2020;8:e000974.
34. Coppola D, Nebozhyn M, Khalil F, et al. Unique ectopic lymph node-like structures present in human primary colorectal carcinoma are identified by immune gene array profiling. Am J Pathol 2011;179:37–45.
35. Nusse R, Clevers H. Wnt/beta-catenin signaling, disease, and emerging therapeutic modalities. Cell 2017; 169:985–999.
36. Sansom OJ, Reed KR, Hayes AJ, et al. Loss of Apc in vivo immediately perturbs Wnt signaling, differentiation, and migration. Genes Dev 2004;18:1385–1390.
37. Lustig B, Jerchow B, Sachs M, et al. Negative feedback loop of Wnt signaling through upregulation of conductin/axin2 in colorectal and liver tumors. Mol Cell Biol 2002; 22:1184–1193.
38. Lee E, Salic A, Kruger R, et al. The roles of APC and Axin derived from experimental and theoretical analysis of the Wnt pathway. PLoS Biol 2003;1:E10.
39. Shankaran V, Ikeda H, Bruce AT, et al. IFNgamma and lymphocytes prevent primary tumour development and shape tumour immunogenicity. Nature 2001; 410:1107–1111.
40. Galon J, Bruni D. Tumor immunology and tumor evolution: intertwined histories. Immunity 2020;52:55–81.
41. Grivennikov SI, Greten FR, Karin M. Immunity, inflammation, and cancer. Cell 2010;140:883–899.
42. Sydora BC, Tavernini MM, Doyle J, Fedorak RN. A defect in epithelial barrier integrity is not required for a systemic response to bacterial antigens or intestinal injury in T cell receptor-alpha gene-deficient mice. Inflamm Bowel Dis 2006;12:750–757.
43. Zhang YG, Wu S, Xia Y, et al. Axin1 prevents Salmonella invasiveness and inflammatory response in intestinal epithelial cells. PLoS One 2012;7:e34942.
44. Bandyopadhyay SK, de la Motte CA, Kessler SP, et al. Hyaluronan-mediated leukocyte adhesion and dextran sulfate sodium-induced colitis are attenuated in the absence of signal transducer and activator of transcription 1. Am J Pathol 2008;173:1361–1368.
45. Wu X, Guo W, Wu L, et al. Selective sequestration of STAT1 in the cytoplasm via phosphorylated SHP-2 ameliorates murine experimental colitis. J Immunol 2012;189:3497–3507.
46. Crncec I, Modak M, Gordziel C, et al. STAT1 is a sex-specific tumor suppressor in colitis-associated colorectal cancer. Mol Oncol 2018;12:514–528.

47. Wang T, Fan C, Yao A, et al. The adaptor protein CARD9 protects against colon cancer by restricting mycobiota-mediated expansion of myeloid-derived suppressor cells. Immunity 2018;49:504–514 e4.
48. Piao JH, Hasegawa M, Heissig B, et al. Tumor necrosis factor receptor-associated factor (TRAF) 2 controls homeostasis of the colon to prevent spontaneous development of murine inflammatory bowel disease. J Biol Chem 2011;286:17879–17888.
49. Bruni D, Angell HK, Galon J. The immune contexture and Immunoscore in cancer prognosis and therapeutic efficacy. Nat Rev Cancer 2020;20:662–680.
50. Mlecnik B, Bindea G, Kirilovsky A, et al. The tumor microenvironment and Immunoscore are critical determinants of dissemination to distant metastasis. Sci Transl Med 2016;8:327ra26.
51. el Marjou F, Janssen KP, Chang BH, et al. Tissue-specific and inducible Cre-mediated recombination in the gut epithelium. Genesis 2004;39:186–193.
52. Chassaing B, Aitken JD, Malleshappa M, Vijay-Kumar M. Dextran sulfate sodium (DSS)-induced colitis in mice. Curr Protoc Immunol 2014;104:15.25.1–15.25.14.
53. Erben U, Loddenkemper C, Doerfel K, et al. A guide to histomorphological evaluation of intestinal inflammation in mouse models. Int J Clin Exp Pathol 2014;7:4557–4576.
54. Trentesaux C, Fraudeau M, Pitasi CL, et al. Essential role for autophagy protein ATG7 in the maintenance of intestinal stem cell integrity. Proc Natl Acad Sci U S A 2020;117:11136–11146.
55. Subramanian A, Tamayo P, Mootha VK, et al. Gene set enrichment analysis: a knowledge-based approach for interpreting genome-wide expression profiles. Proc Natl Acad Sci U S A 2005;102:15545–15550.
56. Sturn A, Quackenbush J, Trajanoski Z. Genesis: cluster analysis of microarray data. Bioinformatics 2002;18:207–208.
57. Fonseka P, Pathan M, Chitti SV, et al. FunRich enables enrichment analysis of OMICs datasets. J Mol Biol 2021;433:166747.
58. Kim E, Tran M, Sun Y, Huh JR. Isolation and analyses of lamina propria lymphocytes from mouse intestines. STAR Protoc 2022;3:101366.
59. Guo Y, Gabola M, Lattanzio R, et al. Cyclin A2 maintains colon homeostasis and is a prognostic factor in colorectal cancer. J Clin Invest 2021;131:e131517.
60. Guinney J, Dienstmann R, Wang X, et al. The consensus molecular subtypes of colorectal cancer. Nat Med 2015;21:1350–1356.

Received March 17, 2022. Accepted October 27, 2022.

Correspondence
Address correspondence to: Christine Perret, PhD or Béatrice Romagnolo, PhD, Inserm U1016, Institut Cochin, 24 Rue du Faubourg Saint-Jacques, 75014 Paris, France. e-mail: christine.perret@inserm.fr or beatrice.romagnolo@inserm.fr.

Acknowledgments
The authors thank S. Robine (Institut Curie, Paris, France), A. Berns (Netherlands Cancer Institute, Amsterdam, The Netherlands), and Anne-Amandine Chassot (University of Nice Sophia Antipolis, Nice, France) for supplying mutant mice. The authors also thank Trinath Jamma (BITS Pilani-Hyderabad Campus, Telangana, India) for help and support for the cell sort at the Flow Core Facility, the staff of the Cochin animal facility, Isabelle Lagoutte from the Imagerie du Vivant facility of Cochin Institute, and Lucie Adoux from the Genomic facility of Cochin Institute.

CRediT Authorship Contributions
Christine Perret, PhD (Conceptualization: Lead; Data curation: Lead; Formal analysis: Lead; Funding acquisition: Lead; Investigation: Lead; Methodology: Lead; Supervision: Lead; Writing – original draft: Lead)
Romain Sanson (Formal analysis: Lead; Investigation: Lead; Methodology: Lead)
Silvia Luna Lazzara (Investigation: Equal; Methodology: Equal)
Caterina Luana Pitasi (Investigation: Supporting; Methodology: Supporting)
David Cune (Investigation: Supporting; Methodology: Supporting)
Coralie Trentesaux (Investigation: Supporting; Methodology: Supporting)
Marie Fraudeau (Investigation: Supporting; Methodology: Supporting)
Franck Letourneur (Methodology: Equal; Software: Equal)
Benjamin Saintpierre (Resources: Lead; Software: Lead)
Morgane Le Gall (Software: Lead)
Pascale Bossard (Methodology: Supporting)
Benoit Terris (Methodology: Equal)
Pascal Finetti (Data curation: Equal; Resources: Equal; Software: Equal)
François Bertucci (Resources: Lead; Software: Lead; Writing – original draft: Supporting)
Emilie Mamessier (Resources: Equal; Software: Lead; Writing – original draft: Supporting)
Béatrice Romagnolo (Conceptualization: Equal; Funding acquisition: Lead; Supervision: Lead)

Data Availability Statement
RNA sequencing data sets are available through the public, open-access repository National Institutes of Health Gene Expression Omnibus platform: =https://www.ncbi.nlm.nih.gov/geo/query/acc.cgi?accGSE196220. GEO accession number: GSE196220.

Conflicts of interest
The authors disclose no conflicts.

Funding
Supported by the National Institute of Health and Medical Research (France), Ligue Contre le Cancer (Equipe Labellisée LNCC 2020), Labex Who Am I? (France; R.S. and C.L.P.), Cancer Research Personalized Medicine, and a Ministère de la Recherche et de l'Enseignement Supérieur fellowship (R.S. and D.C.).